C. Fluvial, Glacial, and Volcanic Interaction

Four papers are attached here, whose results have been summarized in Chapter 16. They are most recent publications, which specifically discuss glacial, possible periglacial, and fluvial landforms partly related or triggered by volcanic activity or by proposed climate changes.

These papers are:

1. Neukum, G; Jaumann, R; Hoffmann, H; Hauber, E; Head, JW; Basilevsky, AT; Ivanov, BA; Werner, SC; van Gasselt, S; Murray, JB; McCord, T (2004) Recent and episodic volcanic and glacial activity on Mars revealed by the High Resolution Stereo Camera *NATURE*, 432 (7020): 971-979.

2. Head, JW; Neukum, G; Jaumann, R; Hiesinger, H; Hauber, E; Carr, M; Masson, P; Foing, B; Hoffmann, H; Kreslavsky, M; Werner, S; Milkovich, S; van Gasselt, S (2005) Tropical to mid-latitude snow and ice accumulation, flow and glaciation on Mars *NATURE*, 434 (7031): 346-351.

3. Murray, JB; Muller, JP; Neukum, G; Werner, SC; van Gasselt, S; Hauber, E; Markiewicz, WJ; Head, JW; Foing, BH; Page, D; Mitchell, KL; Portyankina, G (2005) Evidence from the Mars Express High Resolution Stereo Camera for a frozen sea close to Mars' equator *NATURE*, 434 (7031): 352-356.

4. Hauber, E; van Gasselt, S; Ivanov, B; Werner, S; Head, JW; Neukum, G; Jaumann, R; Greeley, R; Mitchell, KL; Muller, P (2005) Discovery of a flank caldera and very young glacial activity at Hecates Tholus, Mars *NATURE*, 434 (7031): 356-361.

articles

Recent and episodic volcanic and glacial activity on Mars revealed by the High Resolution Stereo Camera

G. Neukum[1], R. Jaumann[2], H. Hoffmann[2], E. Hauber[2], J. W. Head[3], A. T. Basilevsky[1,4], B. A. Ivanov[1,5], S. C. Werner[1], S. van Gasselt[1], J. B. Murray[6], T. McCord[7] & The HRSC Co-Investigator Team*

[1]*Institut fuer Geologische Wissenschaften, Freie Universitaet Berlin, Malteserstrasse 74-100, Bldg D, 12249 Berlin, Germany*
[2]*DLR-Institut fuer Planetenforschung, Rutherfordstrasse 2, 12489 Berlin, Germany*
[3]*Department of Geological Sciences, Brown University, Providence, Rhode Island 02912, USA*
[4]*Vernadsky Institute of Geochemistry and Analytical Chemistry, RAS, Kosygin Street 19, 119991 Moscow, Russia*
[5]*Institute of Dynamics of Geospheres, Leninskiy Prospect 38, 119334 Moscow, Russia*
[6]*Department of Earth Sciences, Open University, Milton Keynes MK7 6AA, UK*
[7]*Hawaii Institute of Geophysics and Planetology, University of Hawaii, 2525 Correa Road, Honolulu, Hawaii 96822, USA*

*A list of all members of the HRSC Co-Investigator team and their affiliations appears at the end of the paper.

The large-area coverage at a resolution of 10–20 metres per pixel in colour and three dimensions with the High Resolution Stereo Camera Experiment on the European Space Agency Mars Express Mission has made it possible to study the time-stratigraphic relationships of volcanic and glacial structures in unprecedented detail and give insight into the geological evolution of Mars. Here we show that calderas on five major volcanoes on Mars have undergone repeated activation and resurfacing during the last 20 per cent of martian history, with phases of activity as young as two million years, suggesting that the volcanoes are potentially still active today. Glacial deposits at the base of the Olympus Mons escarpment show evidence for repeated phases of activity as recently as about four million years ago. Morphological evidence is found that snow and ice deposition on the Olympus construct at elevations of more than 7,000 metres led to episodes of glacial activity at this height. Even now, water ice protected by an insulating layer of dust may be present at high altitudes on Olympus Mons.

On board the European Space Agency (ESA) Mars Express Orbiter, a multiple line scanner instrument, the High Resolution Stereo Camera (HRSC), is acquiring high-resolution colour and stereo images of the surface of Mars[1]. Resolution down to 10 m per pixel coupled with large areal extent (swaths typically 60–100 km wide and thousands of kilometres long) means that small details can be placed in a much broader context than was previously possible. Among the major objectives of the experiment is an assessment of the level of recent geological activity on Mars, particularly the type of volcanic and climate-related deposits that might indicate areas of hydrothermal activity and recent water exchange conducive to exobiological activity.

We have used the new HRSC images and their particular qualities in mapping out terrain types for the interpretation of morphological features and topographic relationships from the three-dimensional data and high-resolution imagery, including the Super Resolution Channel (SRC) data (resolution down to 2.5 m per pixel)[1]. The high-resolution colour data were very useful for distinguishing different materials. The combined use of the HRSC data and nested Mars Orbiter Camera (MOC) or SRC imagery has proven to be extraordinarily helpful in the interpretation of the morphologies and processes that shaped the landforms now visible. Here we focused on the time-stratigraphic relationships and the sequence of events to understand the geological evolution of the martian areas investigated. Time sequences were obtained by determining the number of superimposed impact craters and deriving absolute ages.

This approach has become a powerful tool of planetary studies since the early 1970s, when frequencies of craters per unit area of lunar basaltic lavas were compared with the absolute ages of these lavas determined through isotopic dating of the returned samples and have thus given us a reference scale for interplanetary comparison[2]. These data, along with theoretical modelling and observational data of fluxes of crater-forming impactors for different parts of the Solar System, have made it possible to apply this method to different planets and satellites[3–5]. For this study we used the recently updated cratering chronology model that combines the efforts of two major research groups in this area[5].

The ages from crater counts are limited in accuracy almost exclusively by the statistical error[3]. Other error sources, such as undetected admixtures of secondary craters, volcanic or sublimation pits, are normally minor (<10% of the frequency of superposed craters)[3,5], provided the geological mapping of the areas and the counts are carried out by experienced observers. The statistical errors of individual data points in our counts are mostly <30% (one standard deviation, 1 σ). Because the whole distribution over a wider crater size range is used for fitting the theoretical size–frequency distribution to the measurements, the average statistical error of the data points over the ensemble of measurement is the proper measure for the uncertainty (which, in proportion to the number of data points, is much smaller), resulting in an average uncertainty of 20–30% in frequency. This translates into a 20–30% uncertainty in the absolute ages for ages younger than 3 gigayears (Gyr) and an uncertainty of only 100–200 million years (Myr) for ages older than 3 Gyr. Absolute ages may equally be affected by a possible systematic error of about a factor of two in the crater frequency for an assigned absolute age in the cratering chronology model used. This is due to an uncertainty in the underlying impact flux model used for Mars, relative to the lunar value[4,5].

Time-stratigraphic relationships on martian volcanoes

The Tharsis region of Mars, a huge rise comprising almost 20% of

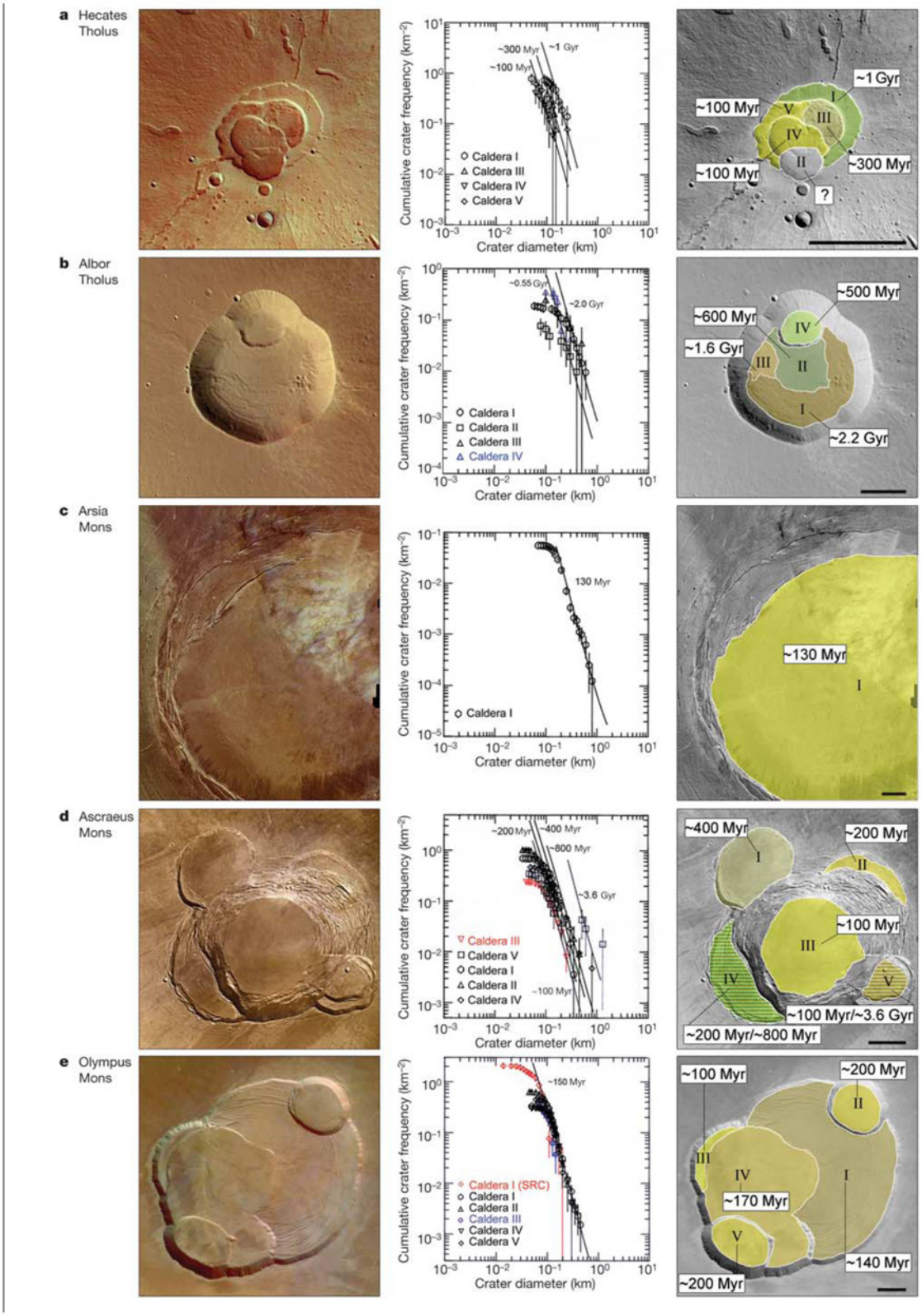

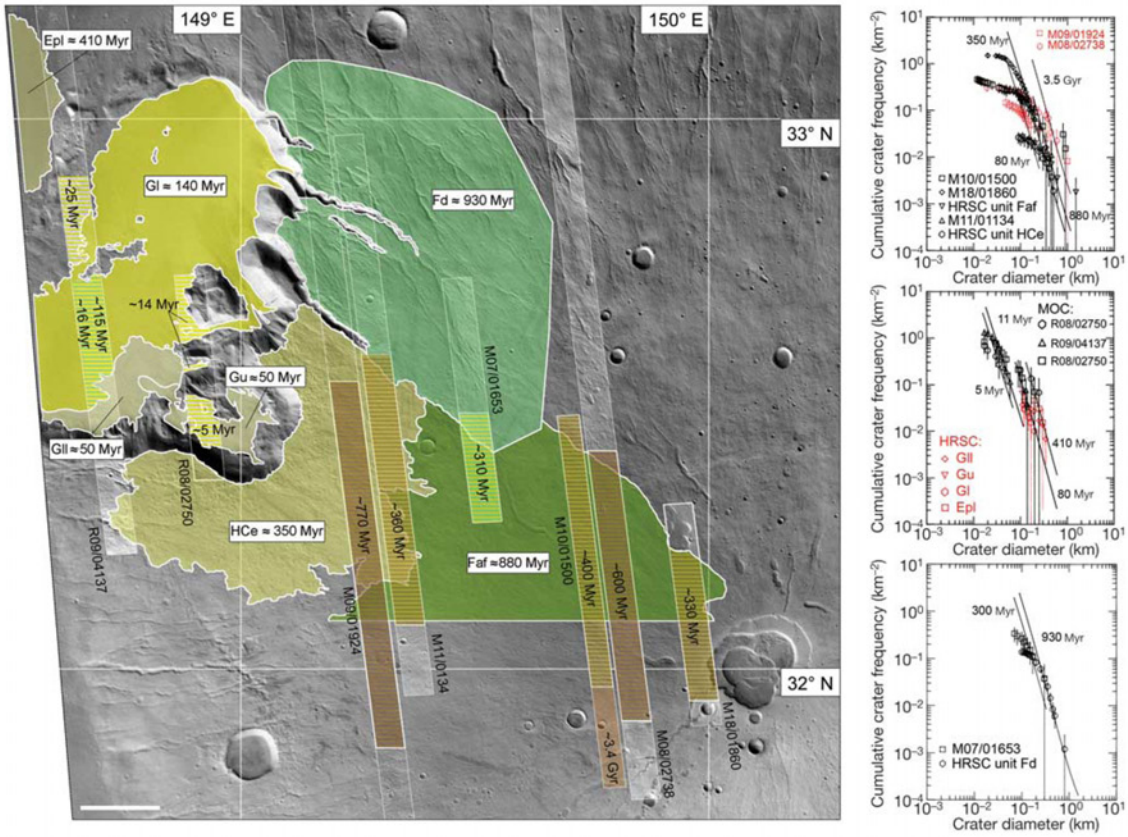

Figure 2 Hecates Tholus counting-area. Base map (HRSC image data and nested MOC data) (left panel), crater size-frequency data and derived absolute ages (three right panels). Methodology as in Fig. 3. Scale bars, 10 km. North is at the top. Error bars, 1-σ error.

the planet, and the smaller Elysium rise have long been known to be the major focal points of volcanism over a significant portion of the history of Mars[6,7]. However, the nature and extent of geologically very recent activity has been unknown. HRSC images acquired in the early phase of the mission (from January to July 2004) have provided broad high-resolution coverage that has cast new light on recent activity. Much of the relatively recent volcanic activity is focused on the summit calderas and flanking rift zones of the major shield volcanoes[8] and therefore these areas were targeted early in the mission. Previous age determinations from crater counting have been limited either by poorer resolution or by the small areas imaged[9].

New HRSC crater counts have confirmed the wide range of ages found earlier[6] for the Tharsis and Elysium volcanism as a whole. For example, the ages of lavas on the flanks of Olympus Mons and Hecates Tholus range between 3,800 and 100 Myr, spanning 80% of the history of Mars (Supplementary Table 1). This extremely long-lived history of volcanic activity is at least two orders of magnitude longer than the typical lifetime of large volcanoes on Earth, which are normally born, grow and become extinct in less than a million years. The very long activity of martian volcanoes implies correspondingly long lifetimes of 'hot spots' in the planet's interior. Hot spots on Earth are estimated to last for 100–200 Myr (ref. 10)—are martian hot spots different from terrestrial ones? Or does plate tectonics on our planet disturb the dynamics or limit our ability to trace back the total lifetimes of Earth's hot spots?

Evidence for geologically young volcanism is abundant in the calderas—depressions commonly found on the summits of volcanic edifices and representing collapses due to magma migration from subsurface reservoirs[11]. The HRSC data show the ages of the floors of different collapse events within calderas on Olympus Mons, Ascraeus Mons, Arsia Mons, Albor Tholus and Hecates Tholus (Fig. 1 and Supplementary Table 1). Most show a complex history, with up to five different collapse episodes detectable, and widely differing ages of the resulting floor deposits (Fig. 1). On Ascraeus Mons, for example (Fig. 1d), the large central caldera floor is ~100 Myr old, and cuts adjacent caldera floors, which are interpreted to have formed ~200, ~400, and ~800 Myr ago, and perhaps earlier. The central caldera floor of Albor Tholus (Fig. 1b) is older than that of Ascraeus (~500 Myr), and is surrounded by portions of older caldera floors dating from ~600, ~1,600 and ~2,200 Myr ago. These findings are in agreement with theoretical analysis, which has suggested that subsurface magma reservoirs must cool and solidify

Figure 1 Investigated volcanic calderas. Base maps (left panels) and counting areas (right panels) of the investigated calderas derived from HRSC data, with crater size-frequency measurements and derived absolute ages (middle panels). Methodology as in Fig. 3. **a**, Hecates Tholus; **b**, Albor Tholus; **c**, Arsia Mons; **d**, Ascraeus Mons; **e**, Olympus Mons. Scale bars, 10 km. North is at the top. Error bars, 1-σ error,

articles

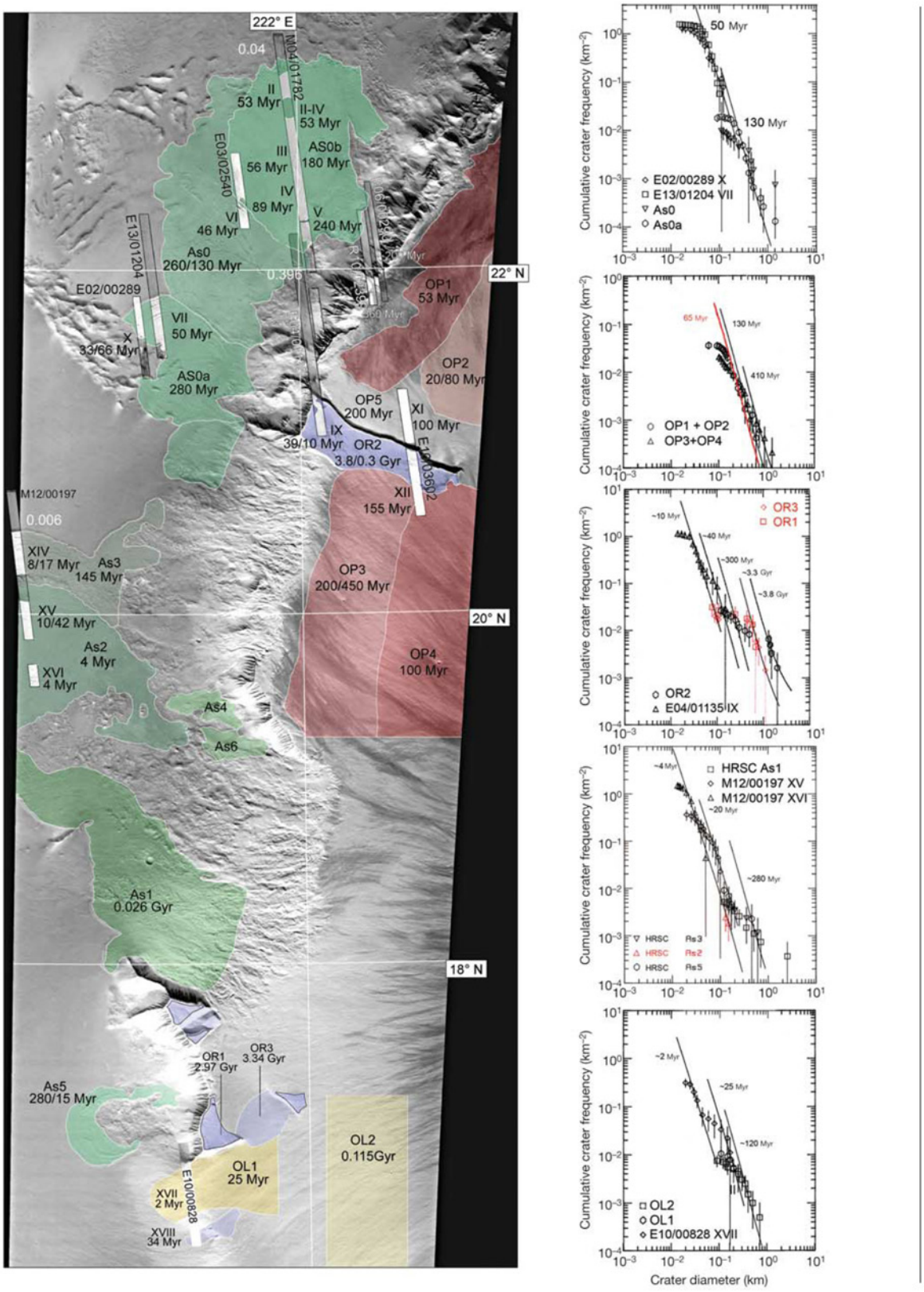

between caldera collapse events, suggesting that magma supply to major shield volcanoes on Mars must have been episodic, rather than continuous[12].

Olympus Mons, however, is unusual by comparison with other calderas. At least five arcuate caldera wall segments can be identified (Fig. 1e), but instead of being spread over hundreds of millions of years in age span, as observed at Ascraeus, Albor and Hecates, the ages of the five Olympus Mons caldera floors cluster in the period 100–200 Myr ago. Theoretically, the ages should be older for high-lying caldera floors and younger for the caldera floors at lower elevation. The different ages are very close to each other within the error limits of ±50 Myr of the age measurements. Thus, the formation of all calderas could have happened in a narrow time span around 150 Myr ago.

It is obvious, however, from the imagery that some of the caldera floors were slightly resurfaced by subsequent thin lava flows or tectonic processes[13] such as horst and graben formation, accompanied by mass wasting processes. Therefore, it is more likely that the calderas formed and were modified subsequently within a period of several tens of millions of years (equivalent to the differences in ages around the average age of 150 Myr). If the theoretical predictions[12] are correct, this implies that separate magma reservoirs were forming, solidifying, and re-forming on timescales averaging perhaps 20 Myr apart. Furthermore, the summit of Arsia Mons is dominated by a single huge caldera whose floor is dated at ~130 Myr ago—falling within the time span represented by the five Olympus Mons ages (~100–200 Myr ago).

These ages confirm some earlier measurements[5,9] on the basis of MOC images in small areas of the calderas of Olympus Mons and Arsia Mons and indicate that the summits of these edifices were very active in essentially the geological present, the last 2–4% of Mars history. These ages provide supporting evidence for the repetitive and episodic nature of caldera formation, and thus magma supply, to the major shield volcanoes on Tharsis and Elysium (compare also with Hecates Tholus in Fig. 2). It is also an interesting coincidence that the summits of four of five of these edifices were very active 100–200 Myr ago, the period in which the crystallization ages of one of two major groups of martian basaltic meteorites fall[14]. This does not necessarily imply a genetic relationship but is a clue suggesting probably widespread volcanic activity on Mars at that time, generating large surface units that the basaltic meteorites may have come from.

It has long been known that the flanking rift zones of the Tharsis Montes and lava flows cascading over the Olympus Mons scarp postdate much of the central edifice-building activity[15]. The new HRSC data permit more precise dating of the duration of activity in these regions. For example, on the lower flanks of Olympus Mons (Fig. 3) are observed flows for which crater size-frequency and age characteristics are interpreted to be representative of activity at ~115 Myr ago, ~25 Myr ago, and with HRSC and MOC data combined, as recently as 2.4 Myr ago.

Figure 3 Olympus Mons western scarp areas. HRSC-image base map with nested MOC data and depiction of the counting areas (left panel) and the resulting ages of the western near-escarpment area of the Olympus Mons volcanic shield, the 7-km-high escarpment and the adjacent plains area to the west with remnants of glacial features (five right panels). The counts show different episodes of resurfacing with erosion of craters and subsequent re-cratering. These episodes and processes are reflected in the different steepnesses of the distributions on the log–log plots, giving a kinked appearance. The flat parts show erosional effects; the steep parts show the re-cratering after the erosional episodes. The martian impact-crater size-frequency distribution[12,13,14] has been fitted to the individual segments of the distribution, giving individual crater-frequency values for the different episodes; by application of the Hartmann–Neukum chronology[14] individual absolute ages can be extracted. In this way it is possible to extract the evolutionary history of the area under investigation in detail. Here the fits to the crater frequencies partly have the character of average isochrons for a group of counts yielding similar numbers. Individual ages may be slightly different and are precisely given in Supplementary Table 1. The errors of the ages are usually around 20–30% for ages younger than 3 Gyr (only 100–200 Myr for older ages) owing to the statistical limitations. The error bars given represent a 1-σ error. In the same way, all ages of less than 2 Gyr may be affected by a possible systematic error of about a factor of two in the cratering chronology model[14] used. North is at the top.

Hydrothermal, fluvial, and glacial activity

Further evidence of very recent and episodic geological activity on Mars has been obtained by HRSC in the form of images and ages of several deposits related to recent climate change. We know that water in the form of ice exists at the polar caps and in the cryosphere of Mars[16], and perhaps locally on the surface[17]. Only recently, however, has it become clear that the extreme variability of the obliquity of the spin axis of Mars and orbit eccentricity[18] can cause significant mobilization of polar volatiles and their redeposition equatorward[19,20]. Of particular interest are the types of deposits that are interpreted to represent the accumulation of water ice in non-polar regions, because these are very sensitive environmental indicators and have important implications for possible life and future automated and human exploration.

For these reasons, early targets for the HRSC instrument were parts of the Elysium region, and the western scarp of the Olympus Mons volcano. On the basis of Viking imagery, channels on the flanks of the Hecates shield have already been detected and interpreted as having been produced by running water[21,22]. We have been able to study the Hecates shield at a resolution of 26 m per pixel in great detail and to determine the ages of some areas using crater-statistics methods (Fig. 2). MOC data were also used, as indicated in Fig. 2. The data show a wide age range over which volcanic activity and related mobilization of water (probably released hydrothermally or partly released through melting of snow caps by volcanically induced heating from underground) with subsequent glacial activity occurred. Here, we present only the gross time-stratigraphic relationships of the development in different areas on the volcano, starting more than 3.4 Gyr ago and shaping the volcano through different episodes of activity (for example, ~900, 400 and 50 Myr ago) until very recent times of about 5 Myr ago. Fluvial and glacial activity can be recognized close to or in the depressions at the northwestern base of the volcano. In southern Elysium, to the southwest of Athabasca Valles, surface features have been observed on the HRSC imagery that look similar to pack-ice on Earth. The age of these deposits is only 5 Myr—in the same range as some of the glacial deposits on Olympus Mons and Hecates Tholus. Details of our findings are supplied elsewhere[23,24].

The other outstanding early target, the Olympus Mons volcano (Figs 3 and 4), is a site known to be characterized by lobate deposits thought to be of glacial origin[17] and recently shown on the basis of the NASA Mars Global Surveyor (MGS) and Odyssey mission data to be a series of lobate rock-covered piedmont glaciers[25]. These deposits are well illustrated in the new HRSC data (Fig. 4b). Therefore, it is now possible to determine more specific ages for them (Fig. 3 and Supplementary Table 1): 130 to 280 Myr for the major lobes, with some subunits in the 20–60 Myr range and locally as young as 4 Myr. These data indicate that the lobate deposits represent several phases of formation, most probably representing periods when significant snow and ice accumulation (possibly accompanied by hydrothermal mobilization of water that flowed down over the edge of the shield, entraining large amounts of non-icy surface material and then freezing) at the Olympus Mons scarp caused mobilization and flow of debris-covered piedmont glaciers into the surrounding low-lying regions.

In several places along the scarp, small linear tongue-like deposits can be seen to emerge from within the apparent accumulation zones of the larger lobate deposits (Fig. 4c). These are interpreted to be

debris-covered alpine glaciers[26] that were previously undetected. Remarkably, the ages of these tongue-like deposits are so young that they cannot be reliably dated because of the lack of craters on them. These smaller tongue-like deposits are interpreted to have formed when conditions were sufficient to cause ice accumulation and local flow, but obviously did not form over the entire extended duration represented by the underlying more widespread deposits. These very young tongue-like deposits are characterized by depressions at the base of the scarp and thus apparently lack an active accumulation zone, suggesting that they are relict features that are no longer forming today.

HRSC and local MOC data reveal evidence for sedimentary

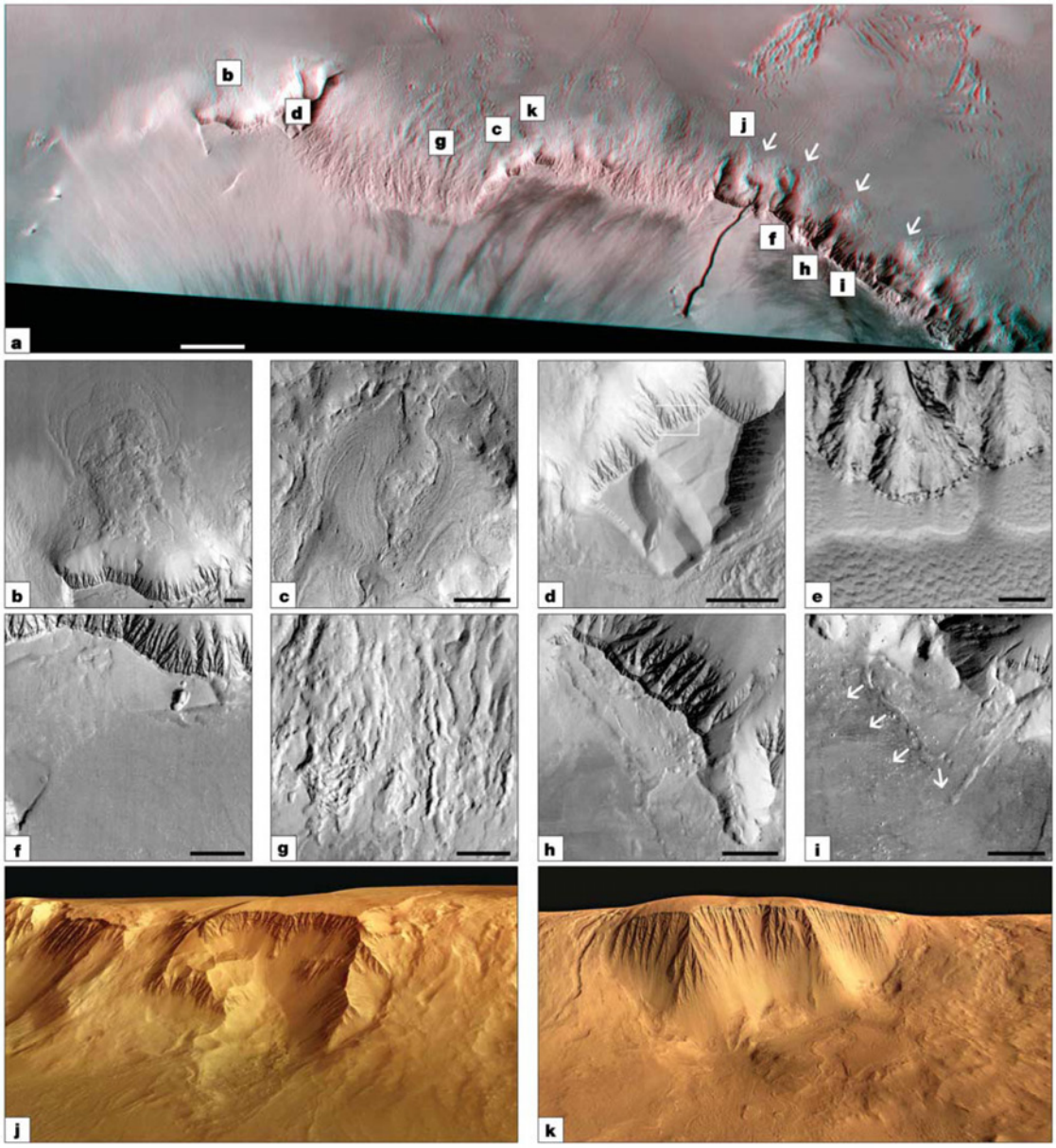

Figure 4 Ice–dust deposits and glaciers on Olympus Mons. **a**, Colour anaglyph for three-dimensional view of the region (scale bar, 30 km); labels b–k indicate designated areas shown on panels b–k (scale bar, 2 km). **b**, Glacier-type lobate flow. **c**, Tongue-like flows. **d**, Mesa at the scarp edge; small white square shows area of panel **e**. **e**, Part of MOC image E05-02498 showing fine layering in the upper part of the mesa material. **f**, Non-impact pits on mesa (upper right) and lava flows entering the mesa (centre left). **g**, Collapse-type depression and channel. **h**, The edge ridge with layers and the upper part of U-shaped valley cut into the ridge and summit plateau. **i**, Glacier-type feature rimmed with small ridges (see arrows). **j**, **k**, Perspective views (from the west) of the western scarp of Olympus Mons showing steep ravined slopes and more gentle slopes with chaos-type depressions in their upper parts, as well as fluvial-type channels and glacier-like flows. The perspective view has been produced through a combination of HRSC nadir and colour image data and the DTM derived from the HRSC stereo data. North is to the right.

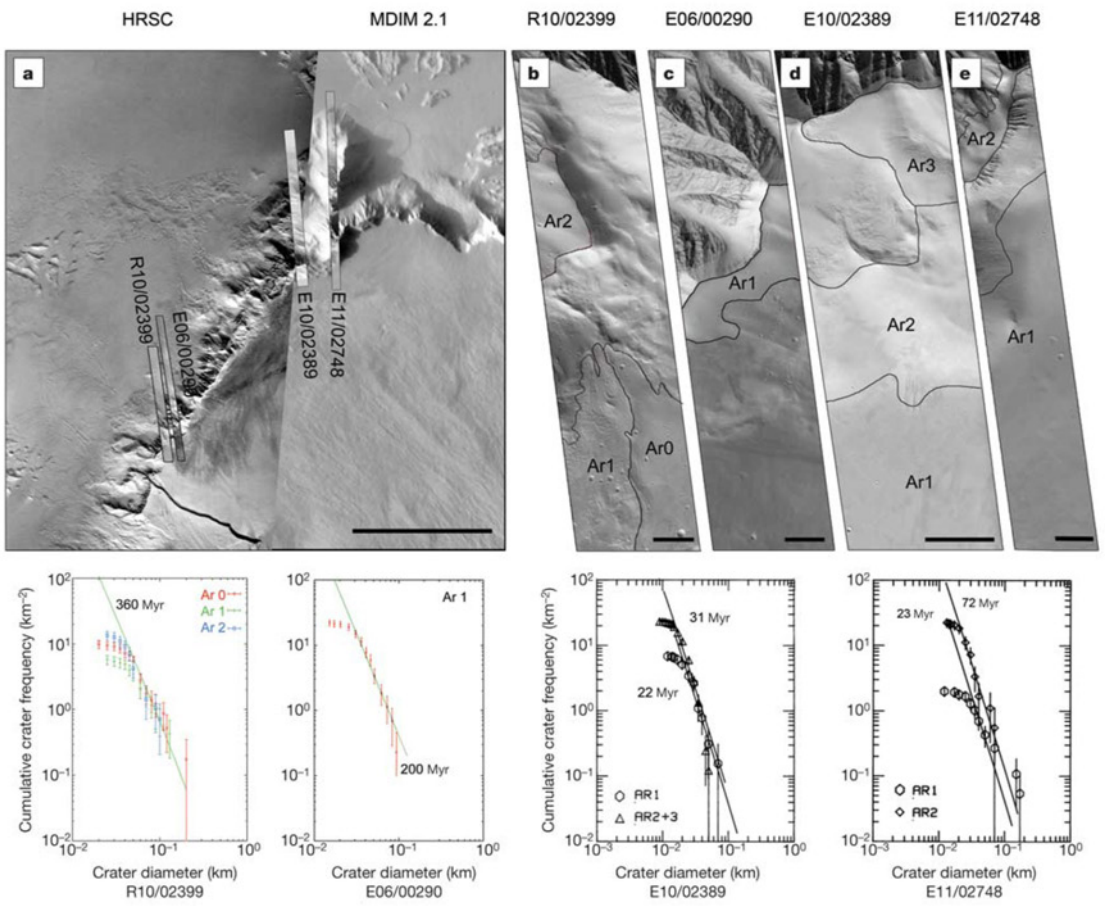

Figure 5 Base map (panels **a**–**e**) and crater statistics (four panels at bottom) of the areas on the northwestern part of Olympus Mons investigated for possible ice–dust coverage and age relationships. **a**, Mosaic of HRSC data (left) and Viking imagery (right) with the location of the MOC images used for morphological study and age determination; scale bar, 50 km. **b**–**e**, MOC images (scale bar, 1 km) with counting areas on flat terrain on the escarpment ridge with its ice–dust cover. **b**, Areas of measurement on MOC image R10/02399 and resulting ages derived from superposed crater frequencies. The ages are roughly the same for all three counting areas on the basis of the fit for intermediate-sized to large craters: 360 Myr with an uncertainty of about 70 Myr. Minor erosion of craters can be recognized in the subtle flattening of the measured distribution in comparison with the fitted theoretical production function. The bending-over characteristics at the small-crater end here and in the other measurements in **c**–**e** stem from loss of craters at the resolution limit of the images. **c**, Areas of measurement on MOC image E06/00290 and resulting age of 200 ± 40 Myr. **d**, Areas of measurement on MOC image E10/02389 and resulting ages of 22 ± 4 Myr and 31 ± 6 Myr. The ages of the individual counting areas AR2 and AR3 have been determined separately with the same results (31 Myr). The AR1 measurements show that some erosion of the ice–dust cover seems to have taken place. **e**, Areas of measurement on MOC image E11/02748 and resulting ages of 23 ± 5 Myr and 72 ± 15 Myr. These ages correlate well with the ages (20 and 80 Myr) measured on adjacent lava flows (OP2 of the base map in Fig. 3). North is at the top. Error bars, 1-σ error.

deposits 50–100 m thick on the rim of the Olympus western scarp, sometimes in the form of mesas (Fig. 4d, e). These optically bright sediments show fine layering obviously different from that which could potentially be formed by accumulation of the lava flows typical of this volcano. We interpret these deposits to represent the remnants of accumulations of dust and ice high on the Olympus construct in previous geological periods. We believe that the presence on some mesas of rimless and deep sinkhole-type depressions (Fig. 4f, upper right) confirms this interpretation. In some places we also see that lava flowing upon these deposits causes their collapse (Fig. 4f, centre left).

Age measurements (Figs 3 and 4) show that the layers formed more than 300 Myr ago, possibly followed by further episodic activity or subsequent major erosional activity until about 65 Myr ago, as seen on the escarpment ridge. Some data for the mesas, from the frequency of some large surviving craters that belong to the underlying substrate, yield age estimates that exceed 3 Gyr. That is close to earlier estimates of the age of the Olympus Aureole, interpreted to have formed by 3.4-Gyr-old gravitation slides of material from the western shield of the Olympus construct[27,28]. This is an indication that the shield of Olympus Mons had already reached heights in excess of 7,000 m very early in its history. The eruption rates must have been very high at the beginning of the growth of the volcano.

Within the broad segments of the upper part of the scarp we observe depressions (Fig. 4g) that are morphologically similar to collapse depressions seen at the source areas of the outflow channels of Mars. The latter are believed to form as a result of release of large

amounts of water from below the surface, for example, the melting of ground ice by magma intrusion[28,29]. Water (subsequently freezing to ice) seems to have been mobilized out of the ground hydrothermally. The collapse-type depressions of the Olympus scarp are also often accompanied by fluvial-type channels, although of relatively small size (Fig. 4h). We interpret these as having been formed by melting ice or ice-and-dust deposits via interaction with lavas.

Glaciers on the shield of Olympus Mons

The edge of the northern part of the scarp is rimmed by a ridge also covered with fine-layered deposits (Fig. 4j, k and Fig. 5a–e). The HRSC-based digital terrain model (DTM) model shows that the ridge stands 400–700 m above the surface adjacent to the east. We interpret the deposits on the ridge as a layer of ice and dust now protected from sublimation by a lag of dust. This 'ice cap' on the ridge formed about 400 Myr ago or earlier, as determined by measuring the superposed crater frequencies as given in Fig. 5. We identify different episodes of subsequent resurfacing of the ice cap at times of 200, 70 and 20–30 Myr ago. We have identified several valleys that are transverse to the ridge and cut into it. In a few cases, the valleys cut back into the summit plateau. The valleys have a U-shaped cross profile and end at the scarp foot with hummocky piles (arrows on Fig. 4a) often having lobate outlines. These are interpreted as debris-covered piedmont glaciers. These characteristics of the valleys suggest that glaciers ploughed them and that the source areas of those glaciers were high on the summit plateau. Moreover, in the potential source area of one of these valleys we see a lobate landform whose orientation suggests glacier movement to the east, towards the volcano centre (Fig. 4i). We estimate the age of this landform—now covered by dust, as are almost all other landforms of the region—to be 200–300 Myr (Figs 3 and 4j). We see evidence of sublimational or eolian degradation significantly erasing the cratering record, which implies that the lobate landform has not been active recently.

The colour data have been examined for effects of the presence of water ice, such as brightening of the surface and possibly flattening of the spectral slope. Colour ratio measurements were done for 16 major terrain types. Brightness in the four HRSC colour channels (centre wavelengths 440, 530, 750 and 970 nm) was calculated by applying the scaling factors from the ground calibration and additional factors derived from comparison with telescopic spectral data[30] and cross-calibration to data from the OMEGA experiment[31]. The measurements showed that the brightness values for each colour channel vary only within a factor of 1.5. All the measured ratios are close to those of "bright regions of Mars"[32] indicating that all the studied terrains are dust-covered. If there is ice, then it appears to be covered and protected from sublimation by a sublimation lag of dust on top of the ice or ice–dust deposit.

The accumulation of ice necessary for developing the high-altitude glaciers and the dust–ice deposits on the mesas and the ridge could have happened at times of high inclination of the planet's spin axis[33]. Experimental data[34] and calculations[35] show that under current climate conditions sun-illuminated water ice (snow) sublimates quickly. But even a thin dust cover shifts the vapour pressure in the pore space to close to the saturation pressure and drastically decreases the sublimation rate of the buried ice[36]. The buried ice (more probably an ice and dust mixture) may be practically stable (slowly sublimating) over millions of years, depending on the diffusive resistance of the upper dust cover against the vapour outflow to the dry atmosphere. Therefore, the layered deposits on the mesas and on the escarpment ridge, and the high-altitude lobate landform may still contain ice. This suggestion may be tested in the future by the MARSIS sounding radar[37] and OMEGA[31,38] experiments on board Mars Express.

Conclusions

The new ages from the HRSC data: (1) confirm the very wide age range (billions of years) over which the Tharsis and Elysium regions were volcanically active; (2) reveal that summit caldera activity was periodic and often consistent with theoretical predictions of magma reservoir cooling and regeneration behaviour; (3) show that the most recent summit caldera activity on the Tharsis volcanoes was clustered ~100–200 Myr ago, practically coinciding with radiometric ages of several martian meteorites; (4) reveal that some of the youngest volcanism on the Tharsis edifices appears to be as young as several million years, thus suggesting that these volcanoes could well erupt in the future; (5) yield evidence for former hydrothermal mobilization of water at the western edge of the Olympus Mons volcano shield and probably on the Hecates Tholus volcano with subsequent development of glaciers; (6) reveal evidence for very young glaciations in the tropical regions of Mars; (7) reveal evidence for deposition of dust and ice and episodes of glaciation high on the Olympus Mons construct; and (8) suggest that water ice may now be present at high altitudes on the edge of the Olympus western scarp. □

Received 3 September; accepted 30 November 2004; doi:10.1038/nature03231.

1. Neukum, G., Jaumann, R. & the HRSC Co-Investigator and Experiment Team. *HRSC—The High Resolution Stereo Camera of Mars Express* 17–35 (European Space Agency Special Publication ESA SP-1240, 2004).
2. Malin, M. C. & Edgett, K. S. Mars Global Surveyor Mars Orbiter Camera: Interplanetary cruise through primary mission. *J. Geophys. Res.* **106,** 23429–23570 (2001).
3. Neukum, G., Ivanov, B. A. & Hartmann, W. K. Cratering record in the inner Solar System in relation to the lunar reference system. *Space Sci. Rev.* **96,** 55–86 (2001).
4. Ivanov, B. A. Mars/Moon cratering rate ratio estimates. *Space Sci. Rev.* **96,** 87–104 (2001).
5. Hartmann, W. K. & Neukum, G. Cratering chronology and the evolution of Mars. *Space Sci. Rev.* **96,** 165–194 (2001).
6. Neukum, G. & Hiller, K. Martian ages. *J. Geophys. Res.* **86,** 3097–3121 (1981).
7. Tanaka, K. The stratigraphy of Mars. *J. Geophys. Res.* **91,** E139–E158 (1986).
8. Greeley, R. & Spudis, P. D. Volcanism on Mars. *Rev. Geophys. Space Phys.* **19,** 13–41 (1981).
9. Hartmann, W. K. *et al.* Recent volcanism on Mars from crater counts. *Nature* **397,** 586–589 (1999).
10. Steinberger, B. Plumes in a convecting mantle: Models and observations for individual hotspots. *J. Geophys. Res.* **105,** 11127–11152 (2000).
11. Crumpler, L. C., Head, J. W. & Aubele, J. C. Calderas on Mars: Characteristics, structure and associated flank deformation. In *Volcano Instability on the Earth and Planets* (eds McGuire, W. J., Jones, A. P. & Neuberg, J.) *Geol. Soc. Spec. Pub.* **110,** 307–348 (1996).
12. Wilson, L., Scott, E. D. & Head, J. W. Evidence for episodicity in the magma supply to the large Tharsis volcanoes. *J. Geophys. Res.* **106,** 1423–1433 (2001).
13. Hauber, E. *et al.* The calderas on Mars—magmatic and tectonic characteristics as revealed through images of the High Resolution Stereo Camera (HRSC) on Mars Express. *Eur. Geophys. Union 1st Gen. Assembly* (abstr.) EGU04-A-07922 (2004).
14. Nyquist, L. E. *et al.* Ages and geologic histories of Martian meteorites. *Space Sci. Rev.* **96,** 105–164 (2001).
15. Crumpler, L. S. & Aubele, J. C. Structural evolution of Arsia Mons, Pavonis Mons and Ascraeus Mons: Tharsis region of Mars. *Icarus* **34,** 496–511 (1978).
16. Carr, M. *Water on Mars* 229 (Oxford Univ. Press, New York, 1996).
17. Lucchitta, B. K. Mars and Earth: Comparison of cold climate features. *Icarus* **45,** 264–303 (1981).
18. Laskar, J. *et al.* Long term evolution and chaotic diffusion of the insolation quantities of Mars. *Icarus* **170,** 343–364 (2004).
19. Richardson, M. I. & Wilson, J. R. Investigation of the nature and stability of the Martian seasonal water cycle with a general circulation model. *J. Geophys. Res.* **107** doi:10.1029/2001JE001536 (2002).
20. Haberle, R. M., Murphy, J. R. & Schaeffer, J. Orbital change experiments with a Mars general circulation model. *Icarus* **162,** 66–89 (2003).
21. Mouginis-Mark, P. J., Wilson, L. & Head, J. W. Explosive volcanism on Hecates Tholus, Mars: Investigation of eruption conditions. *J. Geophys. Res.* **87,** 9890–9904 (1982).
22. Gulick, V. C. & Baker, V. R. Origin and evolution of valleys on Martian volcanoes. *J. Geophys. Res.* **95,** 14325–14344 (1990).
23. Hauber, E. *et al.* Discovery of a flank caldera and very young and glacial activity at Hecates Tholus, Mars, in Mars Express HRSC images. *Nature* (submitted).
24. Murray, J. B. Evidence from the Mars Express High Resolution Stereo Camera for a frozen sea close to Mars' equator. *Nature* (2004) (submitted).
25. Milkovich, S. M. & Head, J. W. Olympus Mons fan-shaped deposit morphology: Evidence for debris glaciers. *6th Int. Mars Conf.* (abstr.) 3149 (2003).
26. Head, J. W. *et al.* Recent ice ages on Mars. *Nature* **426,** 792–802 (2003).
27. Harris, S. A. The aureole of Olympus Mons. *J. Geophys. Res.* **82,** 3099–3107 (1977).
28. Lopes, R., Hiller, K., Neukum, G. & Guest, J. E. Further evidence of the Olympus Mons Aureole. *J. Geophys. Res* **87,** 9917–9928 (1982).
29. Baker, V. R. *The Channels of Mars* (Austin Univ. of Texas Press, Austin, 1982).
30. McCord, T. *et al.* The color capabilities of the Mars Express High Resolution Stereo Camera. *Eur. Geophys. Union 1st Gen. Assembly* (abstr.) EGU04-A-06358 (2004).
31. Bibring, J.-P., *et al. OMEGA: Observatoire pour la Mineralogie, l'Eau, les Glaces et l'Activite.* 37–49 (European Space Agency Special Publication ESA SP-1240, 2004).
32. Banin, A., Clark, B. C. & Waenke, H. in *Mars* (eds Kiefer, H. H., Jakosky, B. M., Snyder, C. W. & Matthews, M. S.) 594–625 (Univ. Arizona Press, Tucson, 1992).

33. Head, J. W. *et al.* Recent mid-latitude glaciation on Mars: Evidence for snow and ice accumulation and flow in Mars Express HRSC data. *Nature* (in the press).
34. Kossacki, K. J., Komle, N. I., Leliwa-Kopystynski, J. & Kargel, G. Laboratory investigation of the evolution of cometary analogs: results and interpretation. *Icarus* **128,** 127–144 (1997).
35. Kossacki, K. J., Markiewicz, W. J., Skorov, Y. V. & Komle, N. I. Sublimation coefficient of water ice under simulated cometary-like conditions. *Planet. Space Sci.* **47,** 1521–1530 (1999).
36. Skorov, Y. V., Markiewicz, W. J., Basilevsky, A. T. & Keller, H. U. Stability of water ice under a porous nonvolatile layer: implications to the south polar layered deposits of Mars. *Planet. Space Sci.* **49,** 59–63 (2001).
37. Picardi, G., *et al. MARSIS: Mars Advanced Radar for Subsurface and Ionosphere Sounding*. 51–69 (European Space Agency Special Publication ESA SP-1240, 2004).
38. Bibring, J. P. *et al.* Perennial water ice identified in the south polar cap of Mars. *Nature* **428,** 627–630 (2004).

Supplementary Information accompanies the paper on **www.nature.com/nature**.

Acknowledgements We thank U. Wolf for help with the crater size-frequency distribution measurements and age evaluation, as well as W. Zuschneid and O. Fabel for their technical assistance and T. Denk for support in the colour data reduction effort. We also thank the ESTEC and ESOC staff, and the DLR Experiment and Operations team, especially T. Roatsch, K.-D. Matz, V. Mertens, J. Flohrer, F. Scholten, and K. Gwinner. J. Korteniemi, M. Aittola, P. Kostama and D. Williams helped with the image planning. This work forms part of the HRSC Experiment of the ESA Mars Express Mission and has been supported by the German Space Agency (DLR) on behalf of the German Federal Ministry of Education and Research (BMBF). Part of the data evaluation is supported by a grant from the German Science Foundation (DFG) within the scope of the priority programme 'Mars and the Terrestrial Planets'.

Competing interests statement The authors declare that they have no competing financial interests.

Correspondence and requests for materials should be addressed to G. N. (gneukum@zedat.fu-berlin.de).

The HRSC Co-Investigator Team (Authors are arranged in alphabetical order) J. Albertz[1], A. T. Basilevsky[2], G. Bellucci[3], J.-P. Bibring[4], M. Buchroithner[5], M. H. Carr[6], E. Dorrer[7], T. C. Duxbury[8], H. Ebner[9], B. H. Foing[10], R. Greeley[11], E. Hauber[12], J. W. HeadIII[13], C. Heipke[14], H. Hoffmann[12], A. Inada[15,18], W.-H. Ip[16], B. A. Ivanov[17], R. Jaumann[12], H. U. Keller[18], R. Kirk[19], K. Kraus[20], P. Kronberg[21], R. Kuzmin[2], Y. Langevin[4], K. Lumme[22], W. Markiewicz[18], P. Masson[23], H. Mayer[7], T. B. McCord[24], J.-P. Muller[25], J. B. Murray[26], F. M. Neubauer[27], G. Neukum (Principal Investigator)[28], J. Oberst[12], G. G. Ori[29], M. Pätzold[27], P. Pinet[30], R. Pischel[12], F. Poulet[4], J. Raitala[31], G. Schwarz[32], T. Spohn[12] & S. W. Squyres[33]

Affiliations for authors: 1, TU Berlin, D-10623 Germany; 2, Vernadsky Institute-RAS, Moscow 117975, Russia; 3, CNR/IFSI, 00133 Rome, Italy; 4, CNRS/IAS, 91405 Orsay cedex, France; 5, TU Dresden, D-01062 Germany; 6, USGS, MS 975 Menlo Park, California 94025, USA; 7, Universität der Bundeswehr München, D-85577 Neubiberg, Germany; 8, JPL, Pasadena, California 91109, USA; 9, TU München, D-80333 Germany; 10, ESTEC/SCI-SR, Postbus 299, NL-2200 AG Noordwijk, The Netherlands; 11, Arizona State University, Box 871404, Tempe, Arizona 85287-1404, USA; 12, DLR, D-12489 Berlin, Germany; 13, Brown University, Box 1846, Providence, Rhode Island 02912, USA; 14, Universität Hannover, D-30167 Germany; 15, Kobe University, 657-8501 Kobe, Japan; 16, National Central University (NCU), Chung-Li 320, Taiwan; 17, IDG-RAS, Moscow 117979, Russia; 18, MPAE, Postfach 20, D-37191 Katlenburg-Lindau, Germany; 19, USGS, Flagstaff, Arizona 86001, USA; 20, TU Wien, A-1040 Wien, Austria; 21, TU Clausthal, D-38678 Clausthal, Germany; 22, University of Helsinki, PO Box 14, SF-00014 Helsinki, Finland; 23, OrsayTerre, F-91405 Orsay Cedex, France; 24, PSI-Nw, Winthrop, Washington 98862, USA; 25, University College London WC1E 6BT, UK; 26, The Open University, Milton Keynes MK7 6AA, Buckinghamshire, UK; 27, Universität Köln, D-50923 Germany; 28, FU Berlin, D-12249, Germany; 29, IRSPS, I-65127 Pescara, Italy; 30, Observatoire de Midi-Pyrénéés, F-31400 Toulouse, France; 31, University of Oulu, FIN-90401 Finland; 32, DLR, D-82234 Wessling, Germany; 33, Cornell University, Ithaca, New York 15853-1301, USA

articles

Tropical to mid-latitude snow and ice accumulation, flow and glaciation on Mars

J. W. Head[1], G. Neukum[2], R. Jaumann[3], H. Hiesinger[1], E. Hauber[3], M. Carr[4], P. Masson[5], B. Foing[6], H. Hoffmann[3], M. Kreslavsky[1], S. Werner[2], S. Milkovich[1], S. van Gasselt[2] & The HRSC Co-Investigator Team*

[1]Department of Geological Sciences, Brown University, Providence, Rhode Island 02912, USA
[2]Institut fuer Geologische Wissenschaften, Freie Universitaet Berlin, Malteserstrasse 74-100, Bldg D, 12249 Berlin, Germany
[3]DLR-Institut fuer Planetenforschung, Rutherfordstrasse 2, 12489, Berlin, Germany
[4]US Geological Survey, MS 975, Menlo Park, California 94025, USA
[5]Orsay-Terre, F-91405, Orsay Cedex, France
[6]ESTEC/SCI-SR, Postbus 299, NL2200AG Noordwijk, The Netherlands
*A list of all members of The HRSC Co-Investigator Team and their affiliations appears at the end of the paper

Images from the Mars Express HRSC (High-Resolution Stereo Camera) of debris aprons at the base of massifs in eastern Hellas reveal numerous concentrically ridged lobate and pitted features and related evidence of extremely ice-rich glacier-like viscous flow and sublimation. Together with new evidence for recent ice-rich rock glaciers at the base of the Olympus Mons scarp superposed on larger Late Amazonian debris-covered piedmont glaciers, we interpret these deposits as evidence for geologically recent and recurring glacial activity in tropical and mid-latitude regions of Mars during periods of increased spin-axis obliquity when polar ice was mobilized and redeposited in microenvironments at lower latitudes. The data indicate that abundant residual ice probably remains in these deposits and that these records of geologically recent climate changes are accessible to future automated and human surface exploration.

Among the most sensitive abiotic indicators of climate change are the accumulation, stability and flow of snow and ice. During the Little Ice Age on Earth (late sixteenth to early twentieth centuries), for example, glaciers at high latitude and altitude advanced an average of several kilometres[1] and today many are receding in concert with warming trends[2]. On Mars, shallow subsurface water-ice stability in the current climate is limited to latitudes higher than about 60°, a theoretical prediction[3] borne out by spacecraft observation[4]. At present the spin-axis obliquity of Mars, thought to be among the major factors in climate change, is about 25°, but calculations show that there were several periods of increasingly higher obliquity in the last several millions of years of the history of Mars[5]. General circulation models show that increased obliquity warms ice-rich polar regions and redistributes water-ice deposits equatorward[6–8]. Indeed, geological observations show evidence for a recent ice age in the last several million years in the form of a latitude-dependent dust–ice mantle extending from high latitudes down to about 30° latitude in both hemispheres[9], and evidence for localized tropical mountain glacier deposits that formed during earlier epochs of the Late Amazonian period on Mars tens to hundreds of millions of years ago[10]. Furthermore, there are numerous morphologic features that might involve ice-rich material at low to mid-latitudes throughout the history of Mars (such as landslides, debris aprons, rock glaciers and piedmont glaciers) but the origins, sources, amounts and state of water in these materials has been controversial[11–20].

Here we report on results from the High Resolution Stereo Camera (HRSC)[21] on board Mars Express that show evidence for (1) the presence of significant volumes of ice and glacial-like flow in massif-marginal deposits at low to mid-latitudes (east of Hellas basin), and (2) very young glacier deposits in equatorial regions (Olympus Mons), suggesting recent climate change. Together these deposits are testimony to the importance and scale of equatorward water redistribution during recent climate change, and to the high likelihood of the presence of significant volumes of buried ice currently in low-latitude regions on Mars.

Glacial-like flow in debris aprons

Debris aprons are a class of geomorphic features seen in mid-latitudes of Mars that are hundreds of metres thick, slope gently away from scarps or highland massifs, terminate at lobate margins, and are interpreted to be viscous flow features of material containing some portion of lubricating ice derived from adjacent highlands[11]. New altimetry and high-resolution images have permitted more comprehensive observations and modelling but have not been able to distinguish conclusively among multiple models of apron formation[17] (for example, ice-assisted rock creep, ice-rich landslides, rock glaciers and debris-covered glaciers) because of our inability to determine the proportion of ice in the rock debris (which can range widely, from ice deposited in debris interstices to debris deposited on ice accumulations)[11–17]. Indeed, different aprons may have different modes of formation.

New HRSC data provide wide coverage of high-resolution data with a high signal-to-noise ratio and stereo capability. Analysis of new HRSC data of a massif-marginal lobe in the eastern Hellas region conclusively shows that the proportion of ice in this deposit was substantial enough to signify glacial and debris-covered glacial activity. Specifically, an 18-km-wide lobe extends about 8 km from the base of a 3.75-km-high massif (Fig. 1). The lobe is up to about 250 m thick, has a convex upward topographic profile, and is separated from the base of the massif by an irregular 50–100-m-deep depression (Fig. 1b, c). A broad alcove in the massif (Fig. 1a) adjacent to the lobe could be interpreted as a landslide scar, representing the source region for the lobate deposit. However, we find several inconsistencies with such an interpretation. For example, within the lobe itself (Fig. 1d), a distal 4-km zone is characterized throughout by a fretted and honeycomb-like texture of irregular pits and ridges. Depressions typically 20–40 m deep

make up 30–40% of this zone and occur between linear moraine-like ridges forming broad convex-outward lobes.

These patterns of sinuous ridges and irregular depressions are unlike landslides and are typical of Earth glacial deposits that remain following debris-containing glacial ice advance, stagnation and ablation[22]. Debris input to glaciers occurs most commonly at ice margins and is thus concentrated along the base of cirques and in medial debris septa that ultimately become medial moraines[23]. Proximal debris addition from rockfalls and increasing debris concentration from below by ice sublimation results in supraglacial debris mantles in the distal direction with great spatial variability in thickness and grain size. As ablation proceeds, debris accumulations represented by englacial septa emerge and form longitudinal or transverse debris ridges separated by areas of cleaner or bare ice. Continued ablation results in the downwasting of the cleaner ice to produce pits, dirt cones and topographic inversion between the ridges, and ultimately the emerging or redistributed debris becomes thick enough to retard further sublimation[24].

The morphological similarities of features observed in Fig. 1 to glacial deposits are thus suggestive of processes of snow and ice accumulation, viscous flows of debris-containing ice, and the subsequent sublimation of significant volumes of the ice in the deposit, leaving behind numerous large sublimation pits tens of metres deep and intervening morainal ridges. Towards the massif, the presence of the linear depression suggests that this may have been the region of snow and ice accumulation; the present depressed topography (with local pits approaching a depth of 100 m) may represent typical proximal high concentrations of ice where more complete sublimation would take place. The presence of numerous plateaus in the fretted part of the deposit suggests that substantial quantities of ice remain beneath a local debris-rich cover, while sublimation has removed intervening ice to produce fretted pits.

These relationships strongly suggest that rather than a landslide scar, the broad alcove represents an accumulation zone for snow and ice that incorporates debris from the massif and under appropriate accumulation conditions, flows out into the surrounding terrain. Although we can see evidence for older lobate deposits, no superposed impact craters have been observed on this deposit, suggesting a geologically recent age for this deposit. Despite its apparent recent age, the evidence for extensive sublimation and wasting are strong indicators that the current environment is not conducive to this large-scale accumulation and flow. However, the probable preservation of ice beneath a substantial portion of this deposit (underlying the sublimation till surface of the inter-pit plateaus) supports the probability that many of the other debris aprons also represent very ice-rich debris-covered glaciers. Indeed, theoretical predictions for Mars imply that dust can insulate buried ice[25] and observations in the Antarctic Dry Valleys suggest that sublimation tills can protect underlying glacial ice for millions of years[26].

Hour-glass-shaped flow in craters

Do other examples of debris aprons show features that might further distinguish between origins from ice-assisted rock creep, ice-rich landslides, rock glaciers and debris-covered glaciers?[11–17] We see further evidence for viscous flow of very ice-rich material in the HRSC data of an hourglass-shaped deposit occurring in two craters at the base of a 3.5–4-km-high massif located on the eastern rim of the Hellas basin (Fig. 2). Two adjacent circular depressions about 9 and 16 km in diameter extend outward from the base of the massif into the surrounding lowlands. In contrast to the previously described deposit, which was oriented with its long axis parallel to the massif slope (Fig. 1), in this location (Fig. 2) the deposit is contained within the craters and appears to fill them. In the proximal crater, the floor is a regionally flat surface that lies nearly at the rim, about 500 m above the surrounding plain, and along a N–S topographic profile (Fig. 2e) the crater appears to be filled nearly to the brim. E–W profiles show, however, that the floor tilts away from the massif at a slope of less than a few degrees (Fig. 2f).

The surface texture on the floor of the crater revealed by the HRSC data (Fig. 2c, d) shows unequivocal evidence for streamlines and lobes typical of ice flow and ice-lobe interaction. Four discrete zones are seen within this crater. To the north, arcuate nested lobes emerge fully developed from the base of the slope and are progressively compressed along the margin; these give way in the north-central part of the crater to a 2.5-km-wide zone of parallel ridges that converge to a narrower 1-km-wide zone where the rim of the

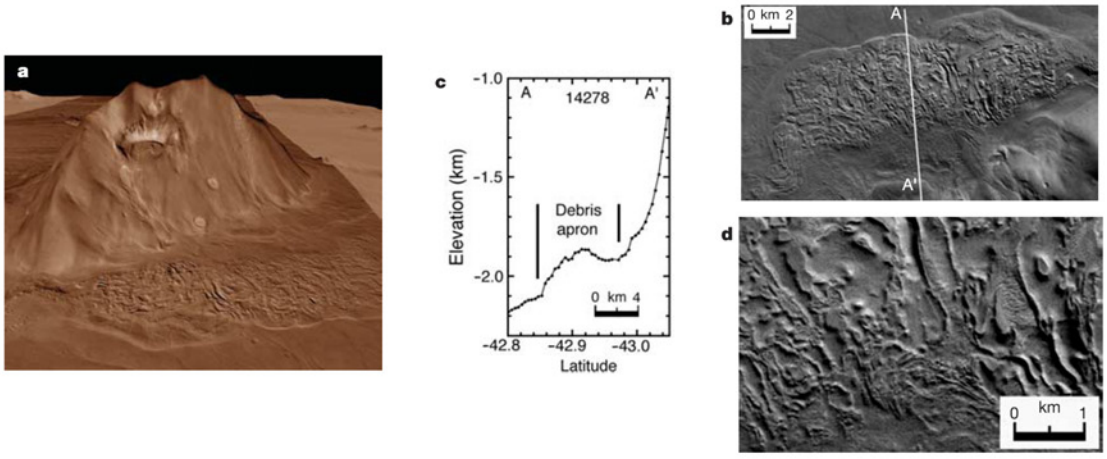

Figure 1 Massif and debris-apron deposits on the eastern rim of the Hellas basin (262.8° W, −43.2°). All images are portions of MEX HRSC Orbit 300. **a**, Perspective view looking east of the 3.75-km-high massif surrounded by debris aprons. Vertical exaggeration is ~30×. **b**, Debris apron with a significant portion comprised of fretted pits and depressions, suggesting the former presence of ice. Line shows location of MOLA profile A–A′. **c**, Altimetric profile across base of massif and debris-apron deposit. MOLA orbit 14278. **d**, Enlargement of portion of fretted debris-apron deposit located just to the right of the profile (Fig. 1b). Note the lobate shapes and the presence of lateral and arcuate ridges and central depressions.

proximal crater is breached. A south central 1.5-km-wide zone of tight arcuate lobes points downslope and becomes compressed into parallel flowlines as it reaches the distal breach. In the southern part of the crater, a 3-km-wide zone of parallel ridges is progressively compressed into a very narrow zone less than 1 km in width. All four of these zones join together at the low point in the crater rim, and flow through a narrow breach less than 2 km wide (Fig. 2d), dropping several hundred metres in elevation and spreading out onto the lower crater floor, creating a set of lobate ridges and depressions further indicative of viscous flow. This configuration is very similar to Earth glacial environments, such as the 60-km-wide Malispina glacier[27], where parallel ridges form due to low-viscosity, high-strain-rate flow in narrow valley glaciers; these then emerge out onto a broad plain and spread out to form a piedmont glacier many times the width of the initial constriction.

The viscous-flow-like crater-filling materials appear to be fully developed at the proximal end of the smaller crater adjacent to the massif alcove (Fig. 2a–d). Here too, the distinctive alcove in the massif could, in principle, represent a landslide scar. Examination of the alcove area details, however, reveals evidence for individual topographic lineations and depressions favouring the accumulation and flow of ice, rather than landslides[20]. In summary, the nature, morphology and topography of the deposit indicates that the alcove served as an accumulation zone for snow and ice that acquired a debris cover from the surrounding steep slopes, and flowed out from the base of the alcove into the surrounding depressions, filling the proximal one and then breaching and overflowing to fill the lower depression. Further evidence that the viscously flowing material was predominantly ice comes from (1) the expanded lobate and complexly deformed nature of the deposit as it spreads out onto the floor of the lower crater from the notch in the upper crater (Fig. 2a, b), (2) the abundance of irregular-shaped pits in the distal lobes, indicating ice sublimation (Fig. 2a, b), (3) evidence for distal moraines around the crater interior margins, indicating ice retreat (Fig. 2b), and (4) compressed and deformed ridges and elongated craters (Mars Orbiter Camera (MOC) image M2300829) also suggest an ice-like rheology (Fig. 2c, d). We thus interpret these features to be debris-covered piedmont-type glaciers.

Young rock glaciers at Olympus Mons

Evidence for extensive debris-covered piedmont glaciers along the northwest edge of the Olympus Mons scarp has been described from Viking and THEMIS data[20,28,29], and together with the tropical mountain glaciers at the Tharsis Montes[10,30], they stand as evidence of extensive localized glaciation in the Late Amazonian when obliquity was typically[5] in excess of 35°. These glaciers extend up to 70–120 km from the base of the Olympus Mons scarp[28,29] and over 350 km from Arsia Mons[10].

HRSC data reveal the presence of several additional rock-glacier-like features along the Olympus Mons basal scarp that are clearly superposed on top of the larger, and thus older, debris-covered piedmont glaciers (Fig. 3). Here the individual lobes are about 25 km in length, and much narrower than the piedmont glacier

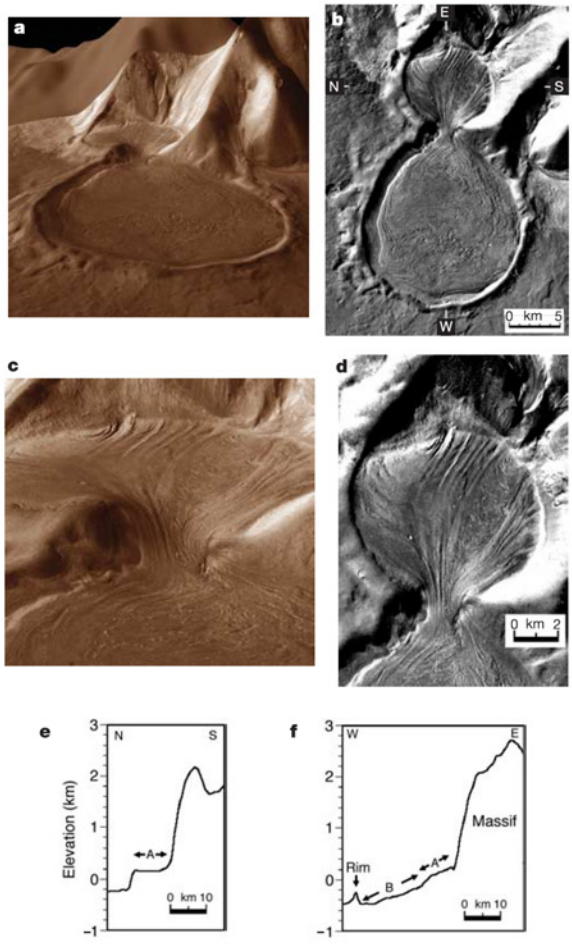

Figure 2 Hourglass-shaped deposit at the base of a massif on the eastern Hellas basin rim (257° W, −39.2°). All images are from MEX HRSC orbit 248. **a**, Perspective view of the 3.5–4-km-high massif showing viscous flow of material from a 9-km crater (marked A in Fig. 2e, f) through a narrow notch into a 16-km-diameter crater (marked B in Fig. 2f). Vertical exaggeration is ~30×. **b**, Vertical view of the two craters showing flowlines and lobes. Tickmarks show the location of MOLA gridded topography profiles in **e** and **f**. **c**, Enlargement of the notch between the two craters showing the four zones where flowlines starting at the base of the slope converge at the narrow 2-km-wide notch and then diverge and spread laterally out into the lobate deposits below. **d**, Perspective view of the proximal crater showing flowlines converging in the gap. MOLA gridded altimetric profiles N–S (**e**) and E–W (**f**).

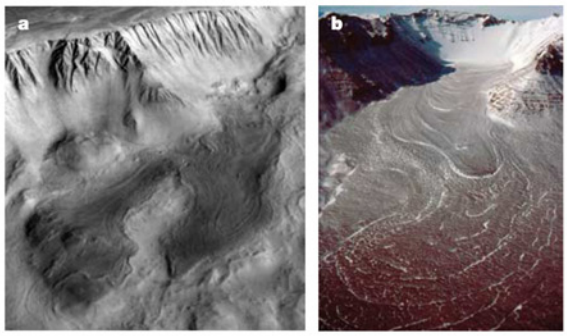

Figure 3 Deposits from a recent lobate rock glacier at the base of the Olympus Mons scarp (138° W, 18°). **a**, Perspective view looking southwest towards the 6-km-high scarp. Note lobate deposits extending about 20–25 km from the base of the alcoves (from right centre towards lower left) darkened for emphasis. HRSC data from MEX orbit 143. **b**, Perspective view of the upper ~5 m of a debris-covered rock glacier emerging from a cirque in Mullins Valley, Antarctic Dry Valleys on Earth. Note the morphologic similarity to features at the base of Olympus Mons. Photo courtesy of David Marchant.

deposit on which they are superposed (Fig. 3a). Furthermore, the paths of the lobes closely follow the topography of the pre-existing deposit, an indication that they are the result of material advancing from the base outward, and not just backwasting and retreat of the residual larger lobe. The sources of the lobes are cuspate alcoves in the basal scarp (Fig. 3a), topographic depressions that are natural traps for wind-blown snow in terrestrial rock glacier environments[31–33] (Fig. 3b). Previously, the broad lobate features had been interpreted to be landslides[34], but terrestrial analogues[20] and new data[10,28–30] have provided very strong evidence for a debris-covered piedmont glacier origin. The new HRSC data add further support to the general glacial interpretation; evidence supporting a rock glacier interpretation for these smaller lobate features includes (1) their origin in alcoves, (2) their elongated subparallel concentric ridges, distorted in relation to underlying and adjacent topography, (3) distinctive terminal moraines, and (4) their strong morphological similarities to terrestrial rock glaciers of known glacial origin[10,30–32] (compare Fig. 3a, b).

Thus, we conclude that there is clear evidence for the formation of recent rock glaciers locally at the base of the Olympus Mons scarp (Fig. 3), similar to typical rock glaciers formed in cirques in the Antarctic Dry Valleys, and their recent advance on Mars to distances measured in several tens of kilometres. The lack of snow in the present alcove, evidence of a depression there, and the presence of fans of scarp talus spreading downslope into these regions with no evidence of gelifluction (the slow downslope movement of sediment associated with seasonal thawing of ground ice), are all evidence that the young rock glaciers are no longer active and that the snow-accumulation conditions that led to their formation no longer persist in this area of Mars.

Role of glaciation in debris-apron origin

Previously, significant controversy surrounded the origin of debris aprons at the base of many massifs on Mars. Outstanding questions focused on (1) the abundance of ice in the deposits during formation, (2) the origin of this ice ('bottom up', from ground ice or groundwater, or 'top down', from atmospheric frost or snow accumulation), and (3) the mode of origin of these features (ranging

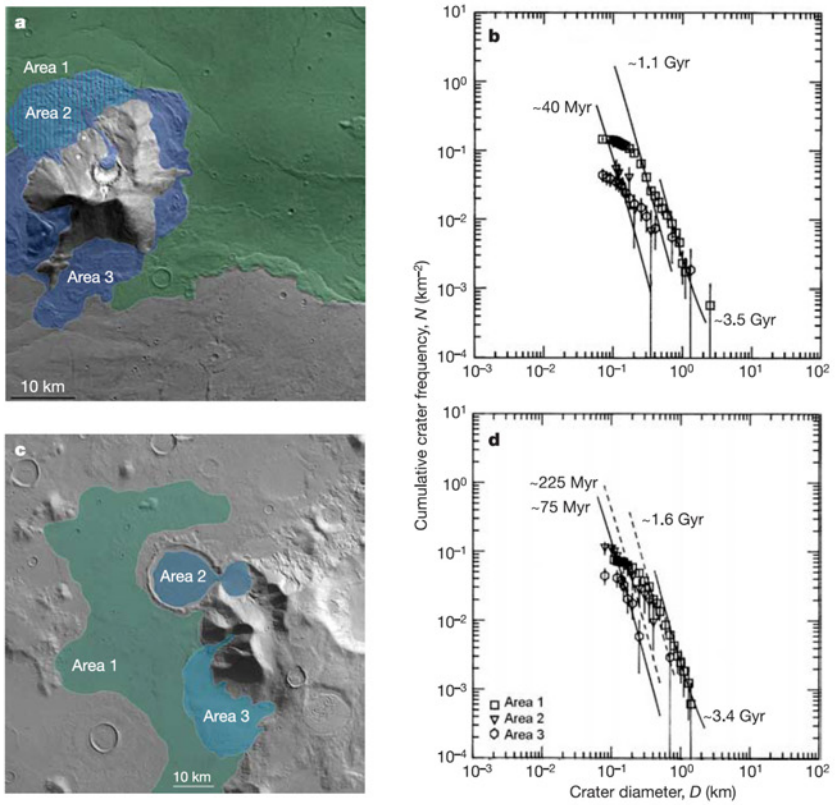

Figure 4 Ages of events in the lobate debris aprons. The impact-crater size-frequency distribution[37–39] has been fitted to individual segments of the distribution, giving values for the different episodes; application of the Hartmann–Neukum cratering chronology provides absolute ages. For ages younger than ~3 Gyr the error is around 20–30%. Error bars are one-sigma. All ages <2 Gyr may be affected in the same way by a possible systematic error of ~2× in the cratering model used[39]. **a**, **b**, Massif and fretted debris apron (**a** and Fig. 1), and impact crater size-frequency distributions (**b**). Area 1, surrounding the massif and lobate deposit, has an age of 3.5 Gyr and appears to have been resurfaced as late as 1.1 Gyr ago, due in part to fluvial activity represented by numerous channels. Debris aprons surrounding the massif (area 3 combined with area 2) display evidence for almost continuous erosion. The portion of the debris apron deposit represented by the fretted debris apron (area 2) is as young as 40 Myr. If debris apron fretting is due to ice sublimation and the sublimation process was continuous over millions of years, some impact craters might be lost and therefore 40 Myr would be a minimum age. Crater distributions are from HRSC orbit 300 data. **c**, **d**, Hourglass structure apron (**c** and Fig. 2), and impact crater size-frequency distributions (**d**). The area surrounding the hourglass and lobate deposit (area 1) has an age of 3.4 Gyr and appears to have been almost continuously resurfaced, with a pause at ~1.4 Gyr, and with some indication of a resurfacing event ending about 225 Myr ago (second dashed line). The hourglass deposit (area 2) and the adjacent debris apron to the south (area 3) have a well-defined age of 75 Myr. Crater distributions from HRSC orbit 248 data.

from ice-assisted rock creep, ice-rich landslides, rock glaciers, to debris-covered glaciers)[11–17]. HRSC data provide important new evidence relevant to each of these outstanding questions. First, the HRSC data support a dominant role for ice in the formation of some of these debris aprons and related deposits with evidence from the pitted terrain indicating very high proportions of ice in a debris apron (Fig. 1b, d), and evidence for low-viscosity flow in the hourglass-like feature, indicating high ice–debris ratios (Fig. 2). Second, evidence for the very high abundance of ice in the deposits and hyperarid cold polar-desert-like conditions during formation argues against bottom-up sources such as groundwater, and favours top-down sources, such as atmospheric-related processes of frost, snow or ice accumulation. Third, the proximity of the source regions for these features to steep-sided debris-covered alcoves, and their close analogue to areas on Earth where snow accumulates to form debris-covered, viscously flowing ice deposits (glaciers) (Fig. 3), strongly suggests that many of these features originate as extremely ice-rich, debris-covered glaciers. The geometry of the features discovered along the base of the Olympus Mons scarp, their similar origin in alcoves, their similarities in size and morphology to terrestrial debris-covered ice-rich rock glaciers, and their direct superposition on larger deposits interpreted to be Late Amazonian debris-covered piedmont glaciers[28,29] all strengthen the interpretation of the potential importance of glacial activity in the formation and evolution of debris aprons surrounding massifs on Mars.

Conclusions and implications

The presence of significant volumes of ice and glacial-like flow in massif-marginal deposits at low to mid-latitudes on Mars (east of Hellas basin; −39° to −43° latitude) and in rock glaciers at the base of Olympus Mons (+18°) strongly suggests that conditions in the geological past have favoured the accumulation of snow and ice and its flow in these tropical and mid-latitude regions. Crater size-frequency distribution data collected from the HRSC images (Fig. 4) of the lobate debris aprons east of Hellas (Figs 1, 2) show evidence for multiple eras of ice-related resurfacing, while the Olympus Mons rock glaciers (Fig. 3) are just a few million years old[35]. Thus, these deposits are further testimony to the importance and scale of equatorward water redistribution during climate change[6–8], and its accumulation in specific areas[35,36]. Furthermore, the superposition of the Olympus Mons rock glaciers on older debris-covered piedmont glacier deposits[28–29], dated at 280 to 130 million years (Myr) ago for the major lobes[36], strongly suggests that these conditions fluctuate with time, and that the geologically very young Olympus Mons rock glaciers documented here (Fig. 3a) represent a recent return to these conditions a few million years ago[36] for periods shorter than those that formed the underlying, much more extensive, Late Amazonian deposits. Finally, that none of these features at present seem to be accumulating ice, and thus flowing and advancing, but instead appear to be undergoing sublimation and wasting, strongly suggests that conditions conducive to their formation are not currently in effect. The latter point is consistent with the idea that Mars may now be in an 'interglacial' period due to its relatively low obliquity[9]. Thus, deposits such as these revealed in detail by the HRSC data provide an important geological record of recent climate change that can be used to test and improve both models of recent climate change[6–8] and predictions of the history of orbital parameters[5]. The lower latitudes of these ice-rich deposits also mean that this key climate record is very accessible to automated and human exploration for direct examination and analysis. □

Received 4 October 2004; accepted 13 January 2005; doi:10.1038/nature03359.

1. Grove, J. M. *The Little Ice Age* (Routledge, London, 1988).
2. Warren, C. R. Glaciers in the greenhouse. *Geogr. Rev.* **8,** 2–7 (1995).
3. Mellon, M. T. & Jakosky, B. M. The distribution and behavior of Martian ground ice during past and present epochs. *J. Geophys. Res.* **100,** 11781–11799 (1995).
4. Feldman, W. C. *et al.* Global distribution of neutrons from Mars: Results from Mars Odyssey. *Science* **297,** 75–78 (2002).
5. Laskar, J. *et al.* Long term evolution and chaotic diffusion of the insolation quantities of Mars. *Icarus* **170,** 343–364 (2004).
6. Richardson, M. I. & Wilson, R. J. Investigation of the nature and stability of the Martian seasonal water cycle with a general circulation model. *J. Geophys. Res.* **107,** doi:10.1029/2001JE001536 (2002).
7. Mischna, M. *et al.* On the orbital forcing of Martian water and CO_2 cycles: A general circulation model study with simplified volatile schemes. *J. Geophys. Res.* **108,** doi:10.1029/2003JE002051 (2003).
8. Haberle, R. M. *et al.* Orbital change experiments with a Mars general circulation model. *Icarus* **161,** 66–89 (2003).
9. Head, J. W. *et al.* Recent ice ages on Mars. *Nature* **426,** 797–802 (2003).
10. Head, J. W. & Marchant, D. R. Cold-based mountain glaciers on Mars: Western Arsia Mons. *Geology* **31,** 641–644 (2003).
11. Squyres, S. W. Martian fretted terrain—Flow of erosional debris. *Icarus* **34,** 600–613 (1978).
12. Colaprete, A. & Jakosky, B. M. Ice flow and rock glaciers on Mars. *J. Geophys. Res.* **103,** 5897–5909 (1998).
13. Mangold, N. & Allemand, P. Topographic analysis of features related to ice on Mars. *Geophys. Res. Lett.* **28,** 407–410 (2001).
14. Mangold, N. *et al.* Experimental and theoretical deformation of ice-rock mixtures: Implications on rheology and ice content of Martian permafrost. *Planet. Space Sci.* **50,** 385–401 (2002).
15. Baratoux, D. *et al.* Evidence of liquid water in recent debris avalanche on Mars. *Geophys. Res. Lett.* **29,** doi:10.1029/2001GL014155 (2002).
16. Mangold, N. Geomorphic analysis of lobate debris aprons on Mars at Mars Orbiter Camera scale: Evidence for ice sublimation initiated by fractures. *J. Geophys. Res.* **108,** doi:10.1029/2002JE001885 (2003).
17. Pierce, T. L. & Crown, D. A. Morphologic and topographic analyses of debris aprons in the eastern Hellas region, Mars. *Icarus* **163,** 46–65 (2003).
18. Kargel, J. S. & Strom, R. G. Ancient glaciation on Mars. *Geology* **20,** 3–7 (1992).
19. Baker, V. R. *et al.* Ancient oceans, ice sheets and the hydrological cycle on Mars. *Nature* **352,** 589–594 (1986).
20. Lucchitta, B. K. Mars and Earth—Comparison of cold-climate features. *Icarus* **45,** 264–303 (1981).
21. Neukum, G. *et al. HRSC: The High Resolution Stereo Camera of Mars Express* 17–35 (Report ESA-SP-1240, European Space Agency Publications Division, Noordwijk, The Netherlands, 2004).
22. Benn, D. I. & Evans, D. J. A. *Glaciers and Glaciation* 237–239 (Arnold, London, 1998).
23. Eyles, N. & Rogerson, R. J. A framework for the investigation of medial moraine formation: Austerdalsbreen, Norway, and Berendon Glacier, British Columbia, Canada. *J. Glaciol.* **20,** 99–113 (1978).
24. Boulton, G. S. in *Till: A Symposium* (ed. Goldthwait, R. P.) 41–72 (Ohio State Univ. Press, Columbus, 1971).
25. Skorov, Yu. V. *et al.* Stability of water ice under a porous nonvolatile layer: implications to the south pole layered deposits of Mars. *Planet. Space Sci.* **49,** 59–63 (2001).
26. Marchant, D. *et al.* Formation of patterned ground and sublimation till over Miocene glacier ice in Beacon Valley, southern Victoria Land, Antarctica. *Geol. Soc. Am. Bull.* **114,** 718–730 (2002).
27. Hartshorn, J. H. Superglacial and proglacial geology of the Malaspina Glacier, Alaska, and its bearing on glacial features of New England. *Geol. Soc. Am. Bull.* **63,** 1259–1260 (1952).
28. Milkovich, S. M. & Head, J. W. Olympus Mons fan shaped deposit morphology: Evidence for debris glaciers. *6th Int. Mars Conf.* abstr. 3149 (2003).
29. Head, J. W., Shean, D. E., Milkovitch, S. M. & Marchant, D. Tropical mountain glaciers on Mars: Evidence for Amazonian climate change. *3rd Mars Polar Conf.* abstr. 8105 (2003).
30. Shean, D. E. *et al.* Tharsis Montes cold-based glaciers: Observations and constraints for modeling and preliminary results. *Lunar Planet. Sci.* **XXXV,** abstr. 1438 (2004).
31. Potter, N. Periglacial geomorphology. *J. Geol. Educ.* **32,** 226–232 (1984).
32. Johnson, P. G. Glacier-rock glacier transition in the southwest Yukon Territory. *Arctic Alpine Res.* **12,** 195–204 (1980).
33. Martin, H. E. & Whalley, W. B. Rock glaciers, part 1, Rock glacier morphology: Classification and distribution. *Prog. Phys. Geogr.* **11,** 260–282 (1987).
34. Morris, E. C. & Tanaka, K. L. *Geologic Maps of the Olympus Mons Region of Mars* (Map I-2327, Misc. Inv. Ser., US Geological Survey, Reston, Virginia, 1994).
35. Neukum, G. *et al.* Recent and episodic volcanic and glacial activity on Mars revealed by the High Resolution Stereo Camera. *Nature* **432,** 971–979 (2004).
36. Hauber, E. *et al.* Discovery of a flank caldera and very young glacial activity at Hecates Tholus, Mars. *Nature* doi:10.1038/nature03423 (this issue).
37. Neukum, G. *et al.* Cratering record in the inner Solar System in relation to the lunar reference system. *Space Sci. Rev.* **96,** 55–86 (2001).
38. Ivanov, B. A. Mars/Moon cratering rate ratio estimates. *Space Sci. Rev.* **96,** 87–104 (2001).
39. Hartmann, W. K. & Neukum, G. Cratering chronology and the evolution of Mars. *Space Sci. Rev.* **96,** 165–194 (2001).

Acknowledgements We thank S. Pratt, A. Cote and J. Dickson for help in data analysis and manuscript preparation, T. Roatsch for data handling, calibration and commanding, F. Scholten and K. Gwinner for photogrammetric processing, and V. Baker for a review. We thank the European Space Agency, DLR (German Aerospace Center), and the Freie Universitaet, Berlin, for their efforts in building and flying the HSRC experiment, and processing the data, and NASA for supporting the participation of J.W.H.

Competing interests statement The authors declare that they have no competing financial interests.

Correspondence and requests for materials should be addressed to J.W.H. (james_head@brown.edu).

The HRSC Co-Investigator Team: J. Albertz[1], A. T. Basilevsky[2], G. Bellucci[3], J.-P. Bibring[4], M. Buchroithner[5], M. H. Carr[6], E. Dorrer[7], T. C. Duxbury[8], H. Ebner[9], B. H. Foing[10], R. Greeley[11], E. Hauber[12], J. W. HeadIII[13], C. Heipke[14], H. Hoffman[12], A. Inada[15,18], W.-H. Ip[16], B. A. Ivanov[17], R. Jaumann[12], H. U. Keller[18], R. Kirk[19], K. Kraus[20], P. Kronberg[21], R. Kuzmin[2], Y. Langevin[4], K. Lumme[22], W. Markiewicz[18], P. Masson[23], H. Mayer[7], T. B. McCord[24], J.-P. Muller[25], J. B. Murray[26], F. M. Neubauer[27], G. Neukum (Principal Investigator)[28], J. Oberst[12], G. G. Ori[29], M. Pätzold[27], P. Pinet[30], R. Pischel[12], F. Poulet[4], J. Raitala[31], G. Schwarz[32], T. Spohn[12] & S. W. Squyres[33]

Affiliations of authors: 1, TU Berlin, D-10623 Germany; 2, Vernadsky Institute-RAS, Moscow 117975, Russia; 3, CNR/IFSI, 00133 Rome, Italy; 4, CNRS/IAS, 91405 Orsay Cedex, France; 5, TU Dresden, D-01062 Germany; 6, USGS, MS 975 Menlo Park, California 94025, USA; 7, Universität der Bundeswehr München, D-85577 Neubiberg, Germany; 8, JPL, Pasadena, California 91109, USA; 9, TU München, D-80333 Germany; 10, ESTEC/SCI-SR, Postbus 299, NL-2200 AG Noordwijk, The Netherlands; 11, Arizona State University, Box 871404, Tempe, Arizona 85287-1404, USA; 12, DLR, D-12489 Berlin, Germany; 13, Brown University, Box 1846, Providence, Rhode Island 02912, USA; 14, Universität Hannover, D-30167 Germany; 15, Kobe University, 657-8501 Kobe, Japan; 16, National Central University (NCU), Chung-Le 320 Taiwan; 17, IDG-RAS, Moscow 117979, Russia; 18, MPAE, Postfach 20, D-37191 Katlenberg-Lindau, Germany; 19, USGS, Flagstaff, Arizona 86001; 20, TU Wien, A-1040 Wien, Austria; 21, TU Clausthal, D-38678 Clausthal, Germany; 22, University of Helsinki, PO Box 14, SF-00014 Helsinki, Finland; 23, Orsay Terre, F-91405 Orsay Cedex, France; 24, PSI-Nw, Winthrop, Washington 98862, USA; 25, University College London WC1E 6BT, UK; 26, The Open University, Milton Keynes MK7 6AA Buckinghamshire, UK; 27, Universität Köln, D-50923 Germany; 28, FU Berlin, D-12249, Germany; 29, IRSPS, I-65127 Pescara, Italy; 30, Observatoire de Midi-Pyrénées, F-31400 Toulouse, France; 31, University of Oulu, FIN-90401 Finland; 32, DLR, D-82234 Wessling, Germany; 33, Cornell University, Ithaca, New York 15853-1301, USA

letters to nature

Evidence from the Mars Express High Resolution Stereo Camera for a frozen sea close to Mars' equator

John B. Murray[1], Jan-Peter Muller[2], Gerhard Neukum[3], Stephanie C. Werner[3], Stephan van Gasselt[3], Ernst Hauber[4], Wojciech J. Markiewicz[5], James W. Head III[6], Bernard H. Foing[7], David Page[1,8], Karl L. Mitchell[9], Ganna Portyankina[5] & The HRSC Co-Investigator Team*

[1]*Department of Earth Sciences, The Open University, Milton Keynes MK7 6AA, UK*
[2]*Department of Geomatic Engineering, University College London, Gower Street, London WC1E 6BT, UK*
[3]*Geosciences Institute, Freie Universität Berlin, Malteserstrasse 74-100, Building D, 12249 Berlin, Germany*
[4]*DLR-Institut für Planetenforschung, Rutherfordstrasse 2, D-12489 Berlin-Adlershof, Germany*
[5]*Max Planck Institute for Aeronomy, Max-Plank-Strasse 2, 37191 Katlenburg-Lindau, Germany*
[6]*Department of Geological Sciences, Brown University, Box 1846, Providence, Rhode Island 02912, USA*
[7]*ESA Research and Scientific Support Department, ESTEC/SCI-SR postbus 299, 2200 AG Noordwijk, The Netherlands*
[8]*Department of Mineralogy, The Natural History Museum, London SW7 5PB, UK*
[9]*Environmental Science Department, Lancaster University, Bailrigg, Lancaster LA1 4YQ, UK*
**A list of all members of The HRSC Co-Investigator Team and their affiliations appears at the end of the paper*

It is thought that the Cerberus Fossae fissures on Mars were the source of both lava and water floods[1,2–4] two to ten million years ago[1,2,5]. Evidence for the resulting lava plains has been identified in eastern Elysium[1,2,4,6–8], but seas and lakes from these fissures and previous water flooding events were presumed to have evaporated and sublimed away[9–11]. Here we present High Resolution Stereo Camera images from the European Space Agency Mars Express spacecraft that indicate that such lakes may still exist. We infer that the evidence is consistent with a frozen body of water, with surface pack-ice, around 5° north latitude and 150° east longitude in southern Elysium. The frozen lake measures about 800 × 900 km in lateral extent and may be up to 45 metres deep—similar in size and depth to the North Sea. From crater counts, we determined its age to be 5 ± 2 million years old. If our interpretation is confirmed, this is a place that might preserve evidence of primitive life, if it has ever developed on Mars.

Extensive fields of large fractured plate-like features on a horizontal surface are visible near the south end of the High Resolution Stereo Camera (HRSC) imaging strip taken on 19 January 2004 (Fig. 1). This area has previously been covered by NASA high-resolution Mars Orbiter Camera (MOC) imagery at pixel sizes down to 1.8 m (Fig. 2). The latter images show fractured plates at a smaller scale. Individual plates are of all sizes from 30 m up to >30 km, with clear signs of break-up, rotation (Fig. 1c) and horizontal drift for distances of several kilometres. The plates show characteristic differences from plate-like features elsewhere on Mars and in the east of Elysium Planitia. The latter features have been interpreted to be rafts of solidified lava floating on the surface of large flood basalts[6], but several observations indicate that this cannot be the case in this area.

Surface ages were determined[12,13] from the size-frequency distribution of 66 impact craters on HRSC images, which suggest a resurfacing event about 5 million years (Myr) ago. Counts of 268 craters on MOC images show that the plates are older than the brighter inter-plate areas (Fig. 3). The statistical errors of the two data sets (counts on plates and inter-plate areas) indicate that they are almost coincident in age, but the whole inter-plate size-frequency distribution falls consistently below that for the plates. This is an indication that the inter-plate areas are really younger than the plates, but within the error limits the age difference could be from a few hundred thousand years up to 2 Myr, with a most likely value of 1 Myr. This age difference is independent of any systematic error in the cratering chronology model used[12,13]. Basalt lava flows 50 m deep can remain partially molten at the centre for only about 5 yr (ref. 14), so these plates cannot be the result of surges and break-outs of lava carrying previously solidified crust, as occurred over timescales of a week or so during the 1783–84 Laki Fissure eruption, Iceland, which is the closest terrestrial analogue to martian flood lavas[6].

Lava break-outs entail build-up and failure of inflating lava to create the plate-like morphology[6], but there are no signs of the inflation that occurs on terrestrial basalts and in other areas of Mars. The Mars Orbiting Laser Altimeter (MOLA) topographic profiles across the area show a remarkably flat surface with broad topography varying by <5 m over more than 60 km, that is, a slope of <0.005°. This compares to a slope of about 0.2° for terrestrial flood basalts.

Furthermore, a drop in surface level occurred after flooding of 18 to 85 m (equivalent to about 9% to 16% of the depth before flooding) within flooded impact craters (Fig. 4). If this had been lava, such a drop would be impossible in these ponded enclosures, because thermal contraction of ponded lava would amount to less than 1% (ref. 15).

Other features in the HRSC image show unique features that provide a clue to their origin. Where the plates have drifted into obstacles, straight or curved lanes have formed downstream within the plates themselves ('L' and 'I' in Fig. 1c). These are not found within lava rafts. Also, the plates are one to two orders of magnitude larger than the largest-known terrestrial basalt rafts. Both these observations, together with the horizontal surface (<0.005°, corresponding to terrestrial tidal sea surface slopes in some estuarine situations) imply an extremely mobile fluid, with characteristics similar to those of water.

Other observations indicate the strong resemblance of these plates to pack-ice. Where pre-existing small topographic highs protrude through the plates to form islands, plate drift has caused rubble piles with pressure ridges on the upstream side (Figs 1c and 2a). Where the highs are craters, these ridges show a superficial resemblance to fluidized ejecta, but unlike the latter, the ridges are subconcentric to the rim and form on one side of the crater only (always the upstream side), show no lobate overlaps or signs of radial movement, have up to 20 subparallel ridges instead of one to three, and show no broad smoother areas proximal to the crater that indicate ejecta flow. Figure 2a shows pressure ridges (denoted 'R') within the rubble pile on the right with wavelengths between 10 and 70 m, which appear to have extended outward from the crater edge as the liquid level dropped and the frozen surface was grounded progressively further down the outer slopes of the crater. These are strikingly similar to rubble piles of sea ice that form around islands in the Arctic and Antarctic (Fig. 2b). The sagging and consequent surface cracking 'C' within the crater itself as the level dropped are also visible. One plate 'F' has drifted into the crater when the level was higher through the gap in the rim 'G', but then become grounded in its present position as the surface lowered, draping it over the northeast rim.

These craters and islands have acted in a similar manner to ice-breakers as the plates drifted past them, leaving straight or curved leads downstream with uniform width (Fig. 1c). The high-resolution MOC image in Fig. 2a shows that these lanes are still very smooth at the 10-m scale, as are similar features in pack-ice on Earth. In places the plates have moved in channels between zones of more stable ice, and overall the direction of drift is towards the west or southwest.

Combinations of processes are unlikely, and have no terrestrial counterparts. Lava plates rafted on mud are not possible because basalt has a density >70% greater than mud. Lava on ice would create pseudocraters, melting and consequent sagging of the raft centres, none of which is observed in this area, and mud rafts floating on mudflows would sink, solid mud having a density 10% greater than fluid mud.

On the basis of this analysis, we interpret the structures and textures to be due to pack-ice formed as a moving and fracturing thermal boundary layer on top of ponded aqueous floodwater that later froze. An early drop in water level occurred while the ice was still drifting (Fig. 2a), mainly owing to evaporation/sublimation, or perhaps seepage of liquid water into the substratum.

Reasonable estimates of the depth can be made by using the rim height to diameter ratios of submerged impact craters. Mean values for simple martian craters are given by: $H = 0.04D^{0.31}$, where H is exterior rim height and D is crater diameter[16]. The impact crater 'I' (Fig. 1c) is 1.1 km in diameter and has only the highest part of the rim exposed, suggesting an initial water depth of about 42 m at that point. Fourteen other crater rims have been identified from their traces partially above or just below the ice as the surface has lowered, yielding initial water depths of between 31 and 53 m, with an average at 45 m. The true depth may be less than these values, as some suspended sediment transported in the early stages would have settled out before freezing. The MOLA profiles across three flooded craters indicate that low parts of the rim are still 0 to 30 m above the mean ice level, suggesting that the evaporation, sublimation and seepage sagging referred to above may have lowered the ice thickness to a present mean depth of around 30 m.

The area lies at the foot of the Athabasca Valles system, where sinuous ridges within the complex of valleys have been likened to those of pack-ice, and plate-like structures there have been proposed to be casts of sediment-rich ice deposited by an ice-rich debris flow, the ice having later sublimed away[17]. Fluvial bedforms also indicate that the Athabasca Valles contained water channels, perhaps fed by a large over-pressured subsurface aquifer[18] giving rise to high

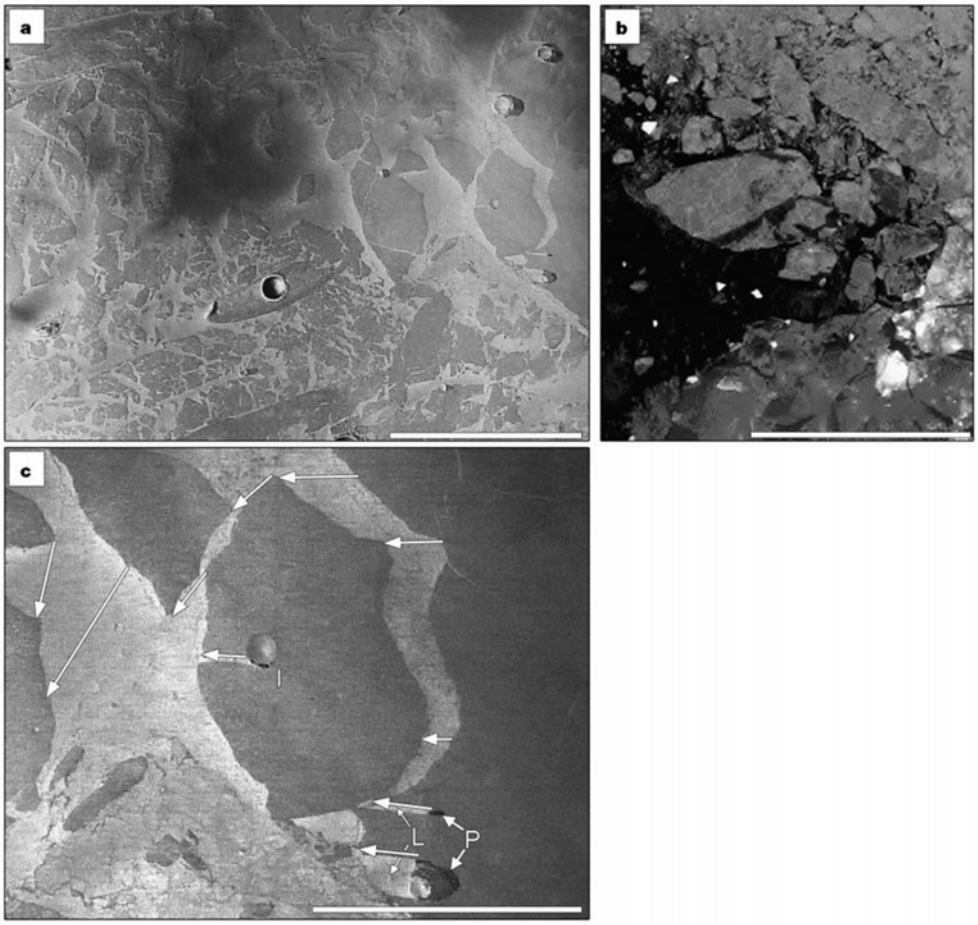

Figure 1 Views of plate-like terrain on Mars, and pack-ice on Earth. **a**, Part of an HRSC image of Mars from orbit 32, with a resolution of 13.7 m per pixel, centred at 5.5° north latitude and 150.4° east longitude, showing plate-like deposits with signs of break-up, rotation and lateral movement to the west-southwest in the lower part of the image. Scale bar is 25 km. **b**, Synthetic Aperture Radar image of pack-ice in the Weddell Sea, Antarctica. Scale bar is 25 km. (ESA image, processed by H. Rott.) **c**, Enlarged view of raft 7 × 12 km showing 8° rotation anticlockwise, causing the clear lane downstream of island 'I' to be curved. Leads 'L' downstream of the crater and small island at lower right are almost straight, indicating unidirectional drift slightly north of westward. Note pressure ridges 'P' upstream of islands. Arrows show relative motion vectors of individual plates. Scale bar is 10 km.

discharge rates[3] of the order of 10^6 m^3 s^2, causing a flood rich in suspended sediment of all sizes.

Water evaporation would be rapid under present Mars conditions[19], but early work[9] indicated that freezing rates at the surface of martian lakes would be of the order of 10^{-5} to 10^{-4} cm s^{-1}, and that surface ice will grow to a thickness of 5–10 m after 1 yr. Freezing will continue until a depth of 50 m is frozen solid in 5–10 yr. Recent work emphasizes that the water should have high concentrations of dissolved salts[20,21], and if it originates from magmatic intrusion, could be several degrees to tens of degrees above freezing on emergence[3]. These factors could produce longer timescales for complete freezing to occur[10], and rapid surface heat loss could cause intense convection that would prevent surface ice formation in the early stages, but allow slush to form.

Ice is unstable at the surface of Mars at present owing to sublimation in the 6-mbar atmosphere, but it is thought that huge volumes of volcanic ash also erupted from Cerberus Fossae[6], which—if contemporaneous with water emission—would have formed a substantial protective layer[22] on the ice. Depending on the porosity and thermal properties of this layer, the subsequent lowering of the floe surfaces could be very slow[23]. Subliming water vapour migrating through the pores will help over time to sinter and chemically bind the particles to form a stronger sublimation lag. To account for the 1-Myr age difference between the plates (pack-ice floes) and the younger lanes in between, we suggest the following sequence of events: first, pack-ice formation with a volcanic ash covering, second, remobilization, break-up and drift of pack-ice, with cessation of volcanic activity, third, freezing of the entire body of water, and finally, the sublimation of the unprotected ice between the ash-covered ice-floes, gradually exposing the suspended sediment at the surface to form a protective layer[22] with a younger age than the floes. Alternatively, the latest Athabasca volcanic activity may be as young as 3 Myr[5], which may have scattered ash that prevented further sublimation of inter-floe areas at this later time. This interpretation is supported by the MOLA profiles, which show them to be up to 3 m lower than the floes.

We do not know whether the frozen body of water is still there, or whether the visible floes are preserved in a sublimation residue draped over the substrate. Two observations suggest that it is still there:

(1) MOLA profiles show that three submerged or partially submerged craters 1.8 to 4.8 km in diameter have depths 2% to 3% of their diameter (Fig. 4), whereas the mean depth of a martian crater of this size range is about 20% of its diameter[16], suggesting that most of the ice is still within the crater, though up to 15% by volume of the crater filling may be suspended sediment. Other submerged craters appear to have similar depths. This point depends on the craters being fresh rather than degraded before

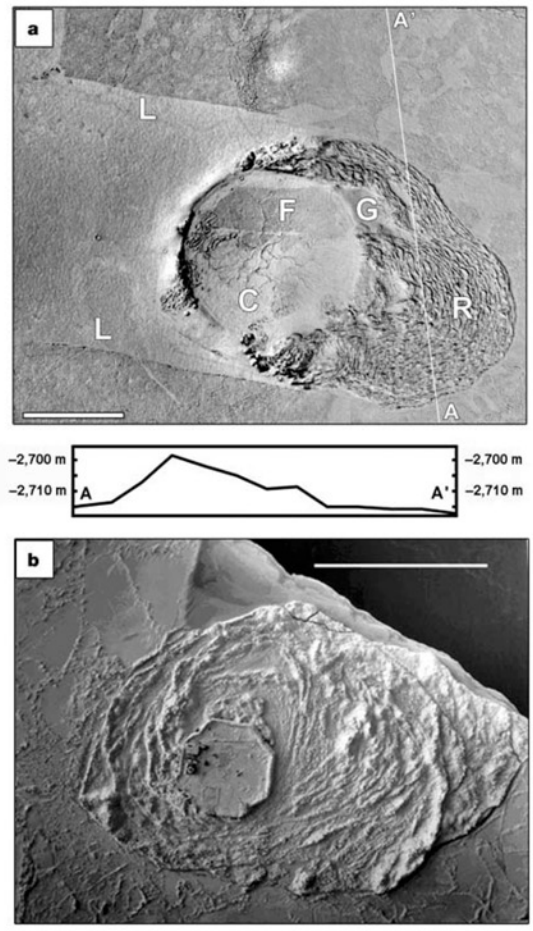

Figure 2 Pressure ridges on Mars, and those caused on Earth by pack-ice drift against obstacles. **a**, High-resolution MOC images E2100112 and R0900475 of an impact crater seen in Fig. 1a. The sides 'L' of the downstream lane are smooth at the 10-m scale, and parallel. The line on the right indicates the MOLA track 19960 crossing the pressure ridges, which are up to 16 m above the surrounding level. The MOLA topographic profile (values in metres) is shown below the image (×60 vertical exaggeration). Scale bar is 1 km. **b**, Air photo of Tarsiut Island, an artificial island in the Beaufort Sea, surrounded by first-year sea ice 1 to 1.5 m thick in the winter of 1983. We note 5-m-high concentric pressure ridging with wavelengths of 2 to 30 m caused by pack-ice rubble becoming grounded on the sloping flanks of the island during winds from different directions. Scale bar is 100 m. (Gulf Canada Resources photo courtesy of T.J.O. Sanderson.) 'C', surface cracking; 'F', a plate that has drifted through a gap 'G' in the rim; 'R', pressure ridges.

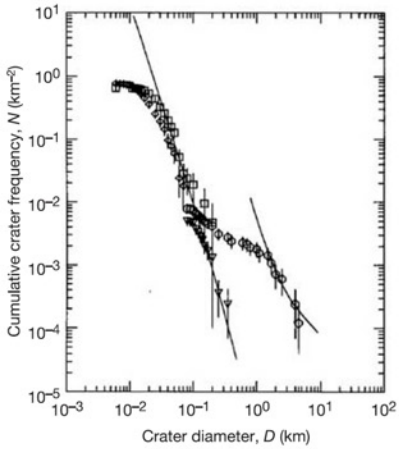

Figure 3 Age dating by crater counting[12,13] on the pack-ice surface using HRSC (triangles) and MOC imagery over a total area of 380 km^2 (squares and diamonds), including those craters that protrude through the surface from the substratum (circles). Whereas the HRSC data indicate a single re-surfacing event about 5 ± 2 million years ago, counts on MOC images show consistently lower numbers for the brighter inter-plate terrain (diamonds) than the darker plate-like terrain (squares) interpreted as ice floes. The lower frequency occurs at all sizes systematically, indicating an age difference of about 1 Myr. The derived age of the substrate before flooding is 3.66 ± 0.05 billion years.

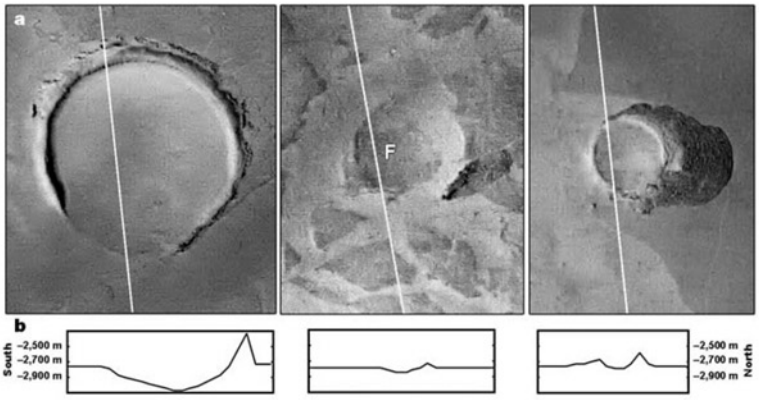

Figure 4 Evidence of ice surface lowering and draping of plate-like features over partly submerged impact craters. MOLA tracks (**a**) and MOLA topographic profiles with 10 × vertical exaggeration (**b**) across three flooded or partially flooded craters 4.8, 2.3 and 1.8 km in diameter from left to right. Values are in metres. Note that the floor sags at least 85, 18 and 25 m respectively, suggesting that 89% to 96% of the proposed ice fill is still within the crater. Note also the raft 'F' draped over the rim and floor of the centre crater. See text for further details.

flooding, but in this area most of the unflooded craters of similar size appear to be fresh with bowl-shaped interiors.

(2) MOLA profiles show a virtually horizontal surface, whereas the ice depth estimates above indicate that the substrate varies in altitude by 55 m. If the ice had been lost, sediment draped over this should have resulted in considerable surface height variation.

Recent work[24,25] has shown that Mars' obliquity, with oscillations of 5° to 10° amplitude and periods of 10^5 yr, was 37° ± 7° between 5 and 10 Myr ago. Global climate model simulations indicate that this would produce a substantially different climate from that of today, with higher dust transport and an atmosphere of higher temperature and pressure[26]. The extremely young age of 5 Myr for the flood suggests that catastrophic flood events from a proposed sub-cryospheric aquifer[20,21] are continuing to happen, as they have done throughout the known history of Mars' surface. The continuous presence of warm water beneath the cryosphere over several billion years might provide more opportunities for life to develop than was once thought. Microorganisms found within deep-sea hydrothermal vent communities[27] are common ancestors to many forms of life on Earth, and the possibility of life developing at similar places elsewhere in the Solar System has been postulated[28]. □

Received 3 September 2004; accepted 18 January 2005; doi:10.1038/nature03379.

1. Berman, D. C. & Hartmann, W. K. Recent fluvial, volcanic and tectonic activity on the Cerberus Plains of Mars. *Icarus* **159,** 1–17 (2002).
2. Burr, D. M., Grier, J. A., McEwen, A. S. & Keszthelyi, L. P. Repeated aqueous flooding from the Cerberus Fossae: Evidence for very recently extant, deep groundwater on Mars. *Icarus* **159,** 53–73 (2002).
3. Head, J. W. III, Wilson, L. & Mitchell, K. L. Generation of recent massive water floods at Cerberus Fossae, Mars, by dike emplacement, cryospheric cracking, and confined aquifer groundwater release. *Geophys. Res. Lett.* **30,** 1577, doi:10.1029/2003GL017135 (2003).
4. Plescia, J. B. Cerberus Fossae, Elysium, Mars: a source for lava and water. *Icarus* **164,** 79–95 (2003).
5. Werner, S. C., van Gasselt, S. & Neukum, G. Continual geological activity in Athabasca Valles Mars. *J. Geophys. Res.* **108,** E12, 8081, doi:10. 1029/2002JE002020 (2003).
6. Keszthelyi, L., McEwen, A. S. & Thordarson, T. Terrestrial analogs and thermal models for Martian flood lavas. *J. Geophys. Res.* **105,** 15027–15049 (2000).
7. Fuller, E. R. & Head, J. W. III Amazonis Planitia: the role of geologically recent volcanism and sedimentation in the formation of the smoothest plains on Mars. *J. Geophys. Res.* **107,** 5081, doi:10.1029/2002JE001842 (2002).
8. Lanagan, P. D. & McEwen, A. S. Cerberus Plains volcanism: constraints on temporal emplacement of the youngest flood lavas on Mars. *6th Int. Conf. on Mars* abstr. 3215 (2003); ⟨http://www.lpi.usra.edu/meetings/sixthmars2003/pdf/3215.pdf⟩.
9. Carr, M. H. Stability of Martian streams and lakes. *Icarus* **56,** 476–495 (1983).
10. Kreslavsky, M. A. & Head, J. W. III Fate of outflow channel effluents in the northern lowlands of Mars: the Vastitas Borealis formation as a sublimation residue from frozen ponded bodies of water. *J. Geophys. Res.* **107,** 5121, doi:10.1029/2001JE001831 (2001).
11. Carr, M. H. & Head, J. W. III Oceans on Mars: an assessment of the observational evidence and possible fate. *J. Geophys. Res.* **108,** 5042, doi:10.1029/2002JE001963 (2003).
12. Hartmann, W. K. & Neukum, G. Cratering chronology and the evolution of Mars. *Space Sci. Rev.* **96,** 165–194 (2001).
13. Neukum, G. *et al.* Recent and episodic volcanic and glacial activity on Mars revealed by the High Resolution Stereo Camera. *Nature* **432,** 971–979 (2004).
14. Patrick, M. R., Dehn, J. & Dean, K. Numerical modelling of lava flow cooling applied to the 1997 Okmok eruption: approach and analysis. *J. Geophys. Res.* **109,** B03202, doi:10.1029/2003JB002537 (2004).
15. Skinner, B. J. Thermal expansion. In *Handbook Of Physical Constants* (ed. Clark, S. P.) *Geol. Soc. Am. Mem.* **97,** 75–96 (1966).
16. Garvin, J. B., Sakimoto S. E. H. & Frawley, J. J. Craters on Mars: global geometric properties from gridded MOLA topography. *Sixth Int. Conf. on Mars* abstr. 3277 (2003); ⟨http://www.lpi.usra.edu/meetings/sixthmars2003/pdf/3277.pdf⟩.
17. Rice, J. W., Parker, T. J., Russel, A. J. & Knudsen, O. Morphology of fresh outflow channel deposits on Mars. *Lunar Planet. Sci. XXXIII* abstr. 2026 [CD-Rom] (Lunar & Planetary Institute, Houston, Texas, 2002).
18. Baker, V. R. *et al.* in *Mars* (eds Kieffer, H. H., Jakosky, B. M., Snyder, C. W. & Matthews, M. S.) 493–522 (Univ. Arizona Press, Tucson, 1992).
19. Wallace, D. & Sagan, C. Evaporation of ice in planetary atmospheres: ice-covered rivers on Mars. *Icarus* **39,** 476–495 (1983).
20. Clifford, S. M. A model for the hydrologic and climatic behavior of water on Mars. *J. Geophys. Res.* **98,** 10973–11016 (1993).
21. Clifford, S. M. & Parker, T. J. The evolution of the Martian hydrosphere: implications for the fate of a primordial ocean and the current state of the northern plains. *Icarus* **154,** 40–79 (2001).
22. Carr, M. H. D/H on Mars: effects of floods, volcanism, impacts and polar processes. *Icarus* **87,** 210–227 (1990).
23. Skorov, Y. V., Markiewicz, W. J., Basilevsky, A. T. & Keller, H. U. Stability of water ice under a porous nonvolatile layer: implications for the south polar layered deposits of Mars. *Planet. Space Sci.* **49**(1), 59–63 (2001).
24. Laskar, J. & Robutel, L. The chaotic obliquity of the planets. *Nature* **361,** 608–612 (1993).
25. Laskar, J., Gastineau, M., Joutel, F., Levrard, B. & Robutel, P. A new astronomical solution for the long term evolution of the insolation quantities of Mars. *Lunar Planet. Sci. XXXV* abstr. 1600 (2004).
26. Haberle, R. M., Murphy, J. R. & Schaeffer, J. Orbital change experiments with a Mars general circulation model. *Icarus* **161,** 66–89 (2003).
27. Humphris, S. E., Zierenberg, R. A., Mullineaux, L. S. & Thomson, R. E. (eds) *Seafloor Hydrothermal Systems* 1–466 (AGU Geophys. Monogr. 91, American Geophysical Union, Washington, DC, 1995).
28. Greenberg, R., Geissler, P., Tufts, B. R. & Hoppa, G. V. Habitability of Europa's crust: The role of tidal-tectonic processes. *J. Geophys. Res.* **105,** 17551–17562 (2000).

Supplementary Information accompanies the paper on **www.nature.com/nature**.

Acknowledgements We thank M. Wählisch for assistance in the MOLA processing and S. Clifford and N. A. Cabrol for criticism that greatly improved the paper.

Competing interests statement The authors declare that they have no competing financial interests.

Correspondence and requests for materials should be addressed to J.B.M. (J.B.Murray@open.ac.uk).

letters to nature

The HRSC Co-Investigator Team: J. Albertz[1], A. T. Basilevsky[2], G. Bellucci[3], J.-P. Bibring[4], M. Buchroithner[5], M. H. Carr[6], E. Dorrer[7], T. C. Duxbury[8], H. Ebner[9], B. H. Foing[10], R. Greeley[11], E. Hauber[12], J. W. HeadIII[13], C. Heipke[14], H. Hoffmann[12], A. Inada[15], W.-H. Ip[16], B. A. Ivanov[17], R. Jaumann[12], H. U. Keller[18], R. Kirk[19], K. Kraus[20], P. Kronberg[21], R. Kuzmin[2], Y. Langevin[4], K. Lumme[22], W. Markiewicz[18], P. Masson[23], H. Mayer[7], T. B. McCord[24], J.-P. Muller[25], J. B. Murray[26], F. M. Neubauer[27], G. Neukum (PI)[28], J. Oberst[12], G. G. Ori[29], M. Pätzold[27], P. Pinet[30], R. Pischel[12], F. Poulet[4], J. Raitala[31], G. Schwarz[32], T. Spohn[12] & S. W. Squyres[33]

Affiliations of authors: 1, TU Berlin, D-10623 Germany; 2, Vernadsky Institute-RAS, Moscow 117975, Russia; 3, IFSI/CNR, Rome, Italy; 4, IAS, Orsay Campus 91405, France; 5, TU Dresden D-01062, Germany; 6, USGS, MS 975 Menlo Park, California 94025, USA; 7, Universität der Bundeswehr München D-85577, Germany; 8, JPL, Pasadena, California 91109, USA; 9, TU München, D-80333 Germany; 10, ESTEC/SCI-SR, Postbus 299, NL-2200 AG Noordwijk, The Netherlands; 11, Arizona State University, Box 871404, Tempe, Arizona 85287-1404, USA; 12, DLR, D-12489 Berlin, Germany; 13, Brown University, Box 1846, Providence, Rhode Island 02912, USA; 14, Universität Hannover, D-30167 Germany; 15, Kobe University, Kobe, Japan; 16, National Central University (NCU) Taiwan; 17, IDG-RAS, Moscow 117979, Russia; 18, MPAE, Postfach 20, D-37191 Katlenburg-Lindau, Germany; 19, USGS, Flagstaff, Arizona 86001, USA; 20, TU Wien, A-1040 Wien, Austria; 21, TU Clausthal, D-38678 Germany; 22, University of Helsinki, PO Box 14, SF-00014 Helsinki, Finland; 23, OrsayTerre, F-91405 Orsay Campus, France; 24, PSI-Nw, Winthrop, Washington 98862, USA; 25, University College London, WC1E 6BT, UK; 26, The Open University, Milton Keynes MK7 6AA, UK; 27, Universität Köln, D-50923 Germany; 28, FU Berlin, D-12249 Germany; 29, IRSPS, I-65127 Pescara, Italy; 30, Observatoire de Midi-Pyrénéés, F-31400 Toulouse, France; 31, University of Oulu, Fin-90401 Finland; 32, DLR, D-82234 Wessling, Germany; 33, Cornell University, Ithaca, New York 15853-1301, USA

Discovery of a flank caldera and very young glacial activity at Hecates Tholus, Mars

Ernst Hauber[1], Stephan van Gasselt[2], Boris Ivanov[3], Stephanie Werner[2], James W. Head[4], Gerhard Neukum[2], Ralf Jaumann[1], Ronald Greeley[5], Karl L. Mitchell[6], Peter Muller[7] & The HRSC Co-Investigator Team*

[1]Institute of Planetary Research, German Aerospace Center (DLR), 12489 Berlin, Germany
[2]Institute of Geosciences, FU Berlin, 12249 Berlin, Germany
[3]Institute for Dynamics of Geospheres, Russian Academy of Sciences, Moscow, 117334, Russia
[4]Department of Geological Sciences, Brown University, Providence, Rhode Island 02912, USA
[5]Department of Geological Sciences, Arizona State University, Tempe, Arizona 85287-1404, USA
[6]Environmental Science Department, Lancaster University, Lancaster LA1 4YQ, UK
[7]Department of Geomatic Engineering, University College London, Gower Street, London WC1E 6BT, UK
**A list of all members of The HRSC Co-Investigator Team and their affiliations appears at the end of the paper*

The majority of volcanic products on Mars are thought to be mafic and effusive[1,2]. Explosive eruptions of basic to ultrabasic chemistry are expected to be common[3,4], but evidence for them is rare and mostly confined to very old surface features[5]. Here we present new image and topographic data from the High Resolution Stereo Camera that reveal previously unknown traces of an explosive eruption at 30° N and 149° E on the northwestern flank of the shield volcano Hecates Tholus. The eruption created a large, 10-km-diameter caldera ~350 million years ago. We interpret these observations to mean that large-scale explosive volcanism on Mars was not confined to the planet's early evolution. We also show that glacial deposits partly fill the caldera and an adjacent depression. Their age, derived from crater counts, is about 5 to 24 million years. Climate models predict that near-surface ice is not stable at mid-latitudes today[6], assuming a thermo-dynamic steady state. Therefore, the discovery of very young glacial features at Hecates Tholus suggests recent climate changes. We show that the absolute ages of these very recent glacial deposits correspond very well to a period of increased obliquity of the planet's rotational axis[7].

The ESA Mars Express mission, an orbiter carrying seven experiments, was inserted into Mars orbit on 25 December 2003. On 19 January 2004, the multiple line scanner instrument, the High Resolution Stereo Camera (HRSC)[8], imaged the volcano Hecates Tholus in the Elysium region. Our study focuses on two overlapping depressions at the northwestern base of Hecates Tholus (Fig. 1) that were mentioned before[9], but without an explanation for their origin. The HRSC image resolution of that area (~26 m per pixel) is better than that of previous images from the Viking Orbiter camera (~40 m per pixel) and from the THEMIS thermal infrared imager (~100 m per pixel). Several very high-resolution images from the Mars Orbiter Camera (MOC) cover small parts of the depressions with 3 to 4 m per pixel. We use digital photogrammetric techniques[10] to derive stereo information with a mean relative point accuracy of ~30 m from the HRSC's multiple line sensors, which observe the surface under different viewing angles.

The smaller of the two depressions (here referred to as 'depression A') has an area of ~12 km × 10 km (Fig. 2a) and a depth between 1,000 and 1,500 m. The northwestern part of its rim is missing where it overlaps with the larger depression (here named 'depression B'). The remaining rim has an elevation between 800 and 1,800 m. The floor is terraced, with an elevation difference of 200–300 m between the two levels. Owing to the incomplete rim, it is difficult to determine its volume. Our best estimate, based on a reconstructed rim, is ~80 km^3. On the flanks of the volcano, an unusual hilly and knobby deposit can be distinguished adjacent to depression A. Its surface is rougher than the rest of the flank's surface, and it extends outward from the rim to a maximum distance of about 15 km.

We favour a volcanic over an impact origin of depression A for four reasons. First, the morphology of the depression, including the two different levels of its floor, is remarkably similar to part of the caldera complex at the shield volcano Ascraeus Mons in the Tharsis region (Fig. 2b), and also to the summit caldera of Hecates Tholus itself (Fig. 2c); impact craters on Hecates Tholus have a distinctly different appearance (Fig. 2d). Second, the stereo information indicates that the walls slope at an average angle of about ~30°, which is steeper than the walls of most martian impact craters[11]. Third, there is no elevated crater rim, which would be expected if depression A were an impact crater. Fourth, the remaining parts of the rim are distinctly not circular, owing to a promontory at the topographically highest part of the rim.

Hence, the cumulative evidence of these independent observations suggests that depression A is volcanic rather than impact-related. There is no evidence for effusive eruptions, for example, lava flows, near depression A. Instead, we interpret the rough material near depression A as the proximal part of pyroclastic materials from an explosive eruption. Relative to the other parts of the flanks, an area between depression A and the summit caldera displays a lack of impact craters and a generally smooth surface texture at the scale of the Viking and HRSC image resolution. It has been interpreted to be a mantling deposit from an explosive eruption at the summit[9]. However, it may as easily have been produced by an explosion at depression A. Indeed, the isolines of the crater density on the western flank of Hecates Tholus (figure 7 in ref. 9) are roughly

concentric around depression A and would be in better agreement with an explosion there than with one at the summit. We interpret the smooth material as the distal part of the erupted pyroclastic material. The presence of many fluvial channels[9,12] may indicate phreatomagmatic (containing magmatic gases and steam) interactions, which could have enhanced the explosivity of the eruption. Crater counts on HRSC and MOC images on both the proximal and distal pyroclastic material, using a new model of cratering

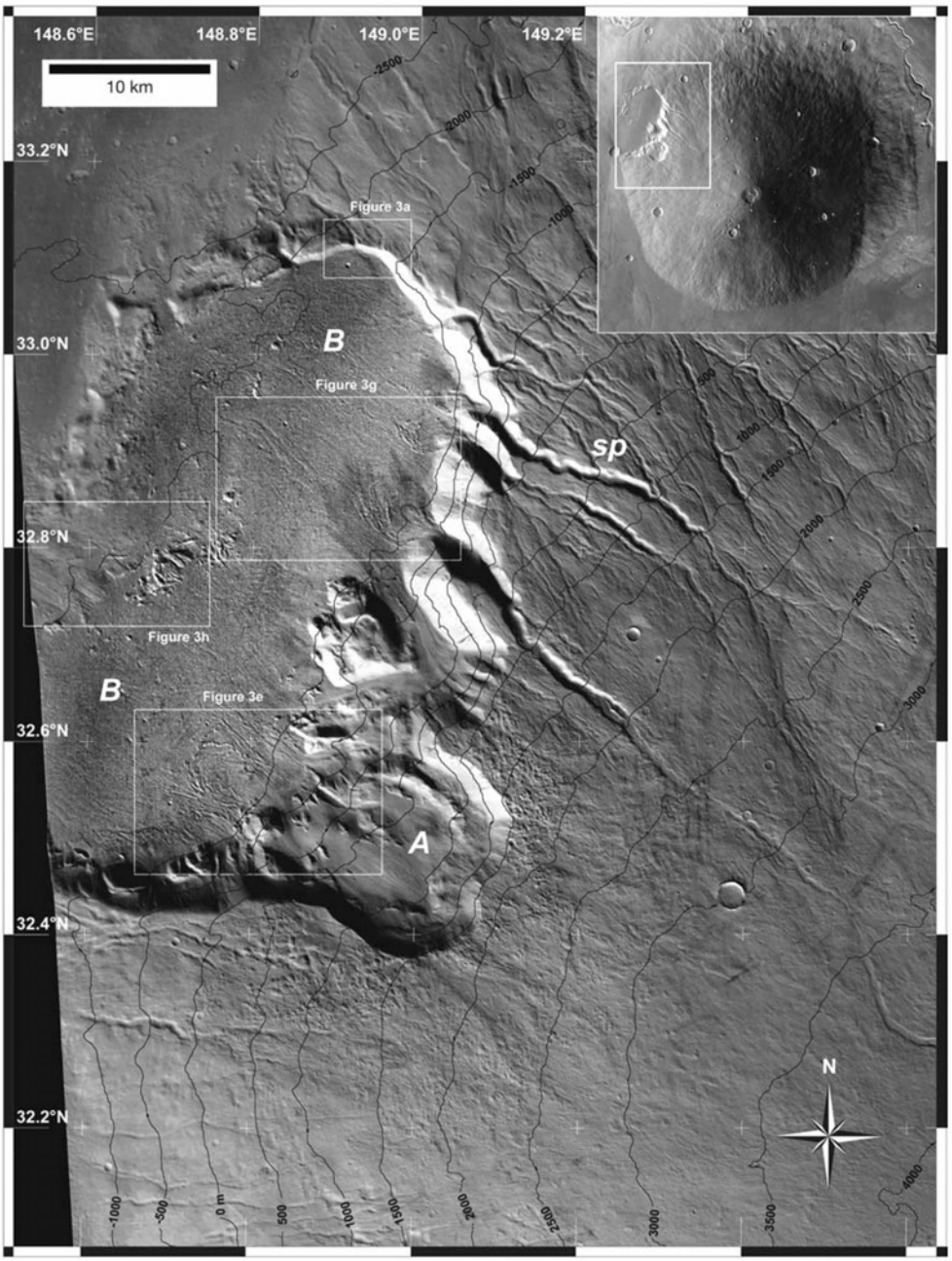

Figure 1 Topographic image map of the study area at the base of the northwestern flank of Hecates Tholus (part of HRSC image h0032_0000.nd). Topographic information (contour line distance 500 m; reference plane is the Mars IAU 2000 ellipsoid) was derived from HRSC stereo imagery. The smaller depression (A) is surrounded by a unique knobby and hilly material. Note the stream piracy pattern (sp) immediately east of a larger depression (B), indicating that an older trend of flow directions was changed as a result of the formation of depression B. The white boxes show the locations of Fig. 3a, e, g and h. The inset on the upper right is a mosaic of Themis-infrared daytime images and shows the location of the base map.

chronology[13,14], give an absolute age for the eruption of ~350 Myr. Hence, large-scale explosive volcanism occurred in the last 10% of the planet's history. This is very young when compared to the several-billion-year-old shields in the highlands, which are among the best-documented examples yet of explosive volcanism on Mars[5].

The shape and distribution of channels near the caldera exhibit several characteristics that shed light on the chronology of volcanic and fluvial processes. East of depression B, we observe two peaks in the azimuthal distribution of the channels. A first set of channels (set A) has an orientation of about N 30° W and is cut off by depression B at several locations. These channels bifurcate and meander where minor surface undulations cause a decrease in flow energy. Several channels that are cut off by depression B can be traced towards the north of the depression, where they seem to continue on its rim. In at least one example (Fig. 3a), the base of a channel starts at a topographically higher level than the floor of depression B, indicating that the channel is older.

A second, younger set of channels (set B) with an azimuthal trend of N 50° W to N 70° W deviates from and partly crosses the older set A, creating a stream piracy pattern. Its channels are deeper and broader than those of set A, and groundwater sapping from a water-rich subsurface might have contributed to their morphology. Set B starts several kilometres away from the eastern rim of depression B, where the topographic gradient becomes higher and is directed towards its rim. The channels follow this topographic trend and deposited large amounts of debris onto the floor. These observations suggest that fluvial activity on Hecates Tholus was continual, not episodic, during the events which formed the depressions, and that the interaction of magma and water or ice may have contributed to the explosive nature of the eruption.

The lower level of depression A and several smaller valleys near the walls of depression B are covered by a smooth deposit, which is lineated in a downslope direction (Fig. 3b). It resembles the lineated valley fill in the fretted terrain near the dichotomy boundary, which has been interpreted as rock glaciers[15,16]. Where the lineated material flows over a topographic step, its surface is distinctively rougher than on flat ground (Fig. 3c). This pattern resembles the change in surface texture encountered at terrestrial icefalls (Fig. 3d). Beyond the topographic step, it extends outward onto the floor of depression B for a distance of ~6 km. It is bounded by curvilinear ridges that resemble terrestrial end moraines (Fig. 3e). Lobate flow features also extend away from the base of the wall for ~2.5 km (Fig. 3f). Where several valleys debouch into depression B, fan deposits extend for up to 6 km on the surrounding plains (Fig. 3g). We interpret them as debris, transported down the strongly incised channels of set B. Alternatively, these deposits could also be moraines. Long and slightly sinuous features extend downslope (~1° slope) from the end of the fan deposits across the entire floor of depression B towards the northwest. We interpret them as distal meltwater channels extending across a proglacial braided outwash plain, analogous to an Icelandic sandur.

A topographic ridge separates depression B from the topographically lower lava flows from Elysium Mons, which are located further towards the northwest. Where this ridge is breached, some rounded, low and shallow hills are superposed by straight, long and narrow ridges and trenches (Fig. 3h). They resemble terrestrial subglacial erosion features (for example, drumlins or whalebacks), and indicate that the glaciation possibly extended beyond depression B towards the northwest. As elsewhere on Mars[17], the strongest arguments for a glacial origin are the assemblage of various surface features that are strikingly similar to terrestrial glacial landforms (medial moraines, end moraines, meltwater channels, drumlins) and their consistently glacial proximal-to-distal relationship (Figs 1 and 3). The volatile most likely to have formed the glaciers is water-ice[17], as the only alternative, CO_2, is particularly unstable at low latitudes under any conceivable atmospheric conditions. The water source could have been precipitation or groundwater that freezes when coming into contact with ice. Precipitation of water on the martian surface is known to take place even under the current thin atmosphere[18]. There are no obvious surficial pathways of water into depression A. Hence, groundwater emerging at the base of scarps bounding the depressions might have fed the glaciers in depression A. However, the local microenvironment at the floors of the depressions, which are partly protected from insolation by steep walls, might act as a cold trap to enhance frost deposition as a water source.

We performed crater counts on HRSC and MOC images of the glacial features shown in Fig. 3, and obtained cratering model[14] ages between ~25 and 5 Myr (Fig. 4). The detection of very young glacial features at a latitude of 30° N in the Elysium region has profound implications for the recent martian climate history. Geologic observations suggest that Mars has experienced recent ice ages[19,20], and it is inferred from gamma-ray and neutron spectroscopy that water might indeed be present today near the surface[21]. However,

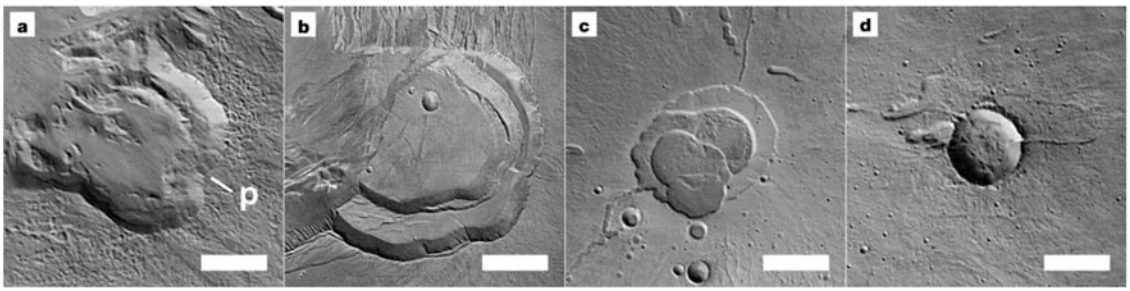

Figure 2 Morphology of calderas. **a**, Feature interpreted to be a caldera on the northwestern flank of Hecates Tholus (depression A of Fig. 1). Owing to a promontory (p), the outline is distinctively non-circular, making an impact origin improbable. Note the two levels of floor elevation, with lineations in the SE–NW direction filling the lower level. **b**, Part of the summit caldera complex of Ascraeus Mons (part of HRSC image h0068_0000.nd, taken on 31 January 2004; centre at 11.13° N, 255.95° E). Note the two levels of floor elevation, similar to what is observed in depression A. **c**, Summit caldera of Hecates Tholus (32.05° N, 150.1° E). Note the morphologic similarity of this caldera and the calderas shown in **a** and **b**. **d**, The largest impact crater on Hecates Tholus (32.28° N, 150.8° E) displays a sharp, elevated crater rim and a continuous floor that is not divided into two elevation levels. Note the overall dissimilarity with **a**, **b** and **c**. In all images, North is up and the white scale bar is 5 km. Figures 2a, c and d are details of HRSC h0032_0000.nd.

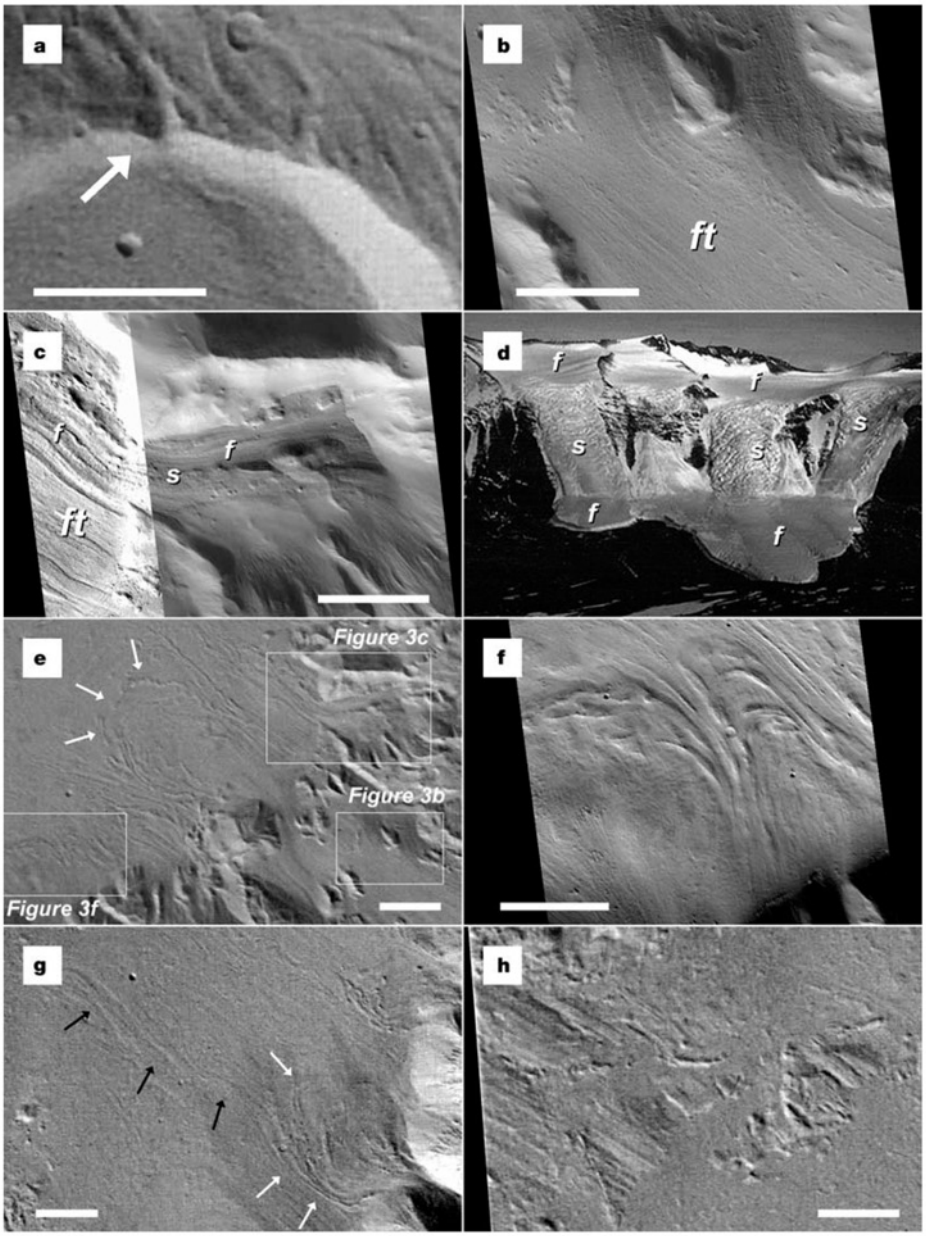

Figure 3 Surface landforms indicative of fluvial and glacial processes at the northwestern flank of Hecates Tholus. **a**, A valley cut upstream by depression B resembles a hanging valley, although true hanging valleys are cut downstream by other valleys. The valley predates the depression (see Fig. 1 for location). **b**, Lineated material (ft), resembling terrestrial medial moraines. A similar surface texture is observed at the fretted terrain[15,16] (MOC image R0802750; see Fig. 3e for location). **c**, Lineated material flowing over the topographic step between depressions A (higher, left) and B (lower, right). Where the topographic gradient is steep (s), the surface texture is rougher than on flat terrain (f), resembling the change in texture observed in terrestrial icefalls (compare with Fig. 3d; MOC images M03-01763 and R08-02750; see Fig. 3e for location). **d**, Icefalls in Taylor Valley, Antarctica (77° 45′ S, 162° 30′ E). Note the change in surface texture between flat (f) and steep (s) terrain, similar to Fig. 3c. Photo courtesy of T. Lowell. **e**, Curvilinear, moraine-like features (white arrows) downslope of the topographic scarp between depressions A and B (see Fig. 1 for location; white boxes show location of Figs 3b, c and f). **f**, Lobate flow features near the base of the wall of depression B, resembling glacial flow features on Earth (MOC image R09-04137; see Fig. 3e for location). **g**, Fan deposits (white arrows) in depression B at the terminations of deeply incised valleys. Faint and slightly sinuous features (black arrows) indicate water runoff from the deposits (see Fig. 1 for location). **h**, Low, rounded hills with superposed long and thin ridges, similar to terrestrial subglacial erosion features (see Fig. 1 for location). Scale bars in Fig. 3a, e, g and h (all part of HRSC image h0032_0000.nd) are 2 km, and in Fig. 3b, c and f are 1 km.

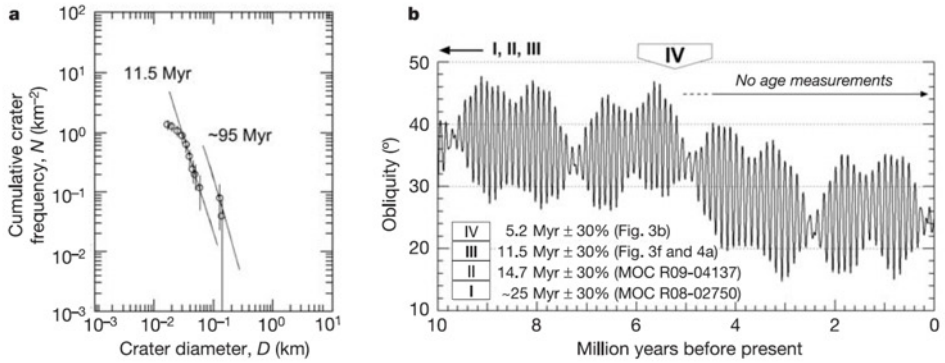

Figure 4 Chronology of glacial surface features and correlation to obliquity changes. **a**, Crater size-frequency distribution for the floor of depression B as observed in MOC R09-04137. Crater model curves according to a new cratering chronology model[13] are fitted to the measurements. The crater model age is 11.5 Myr. An older crater population (right curve) corresponds to an age of ~95 Myr, which might be associated with an older episode of glaciation. Additional ages of 5.2, 14.7 and ~25 Myr were obtained from other MOC images (Fig. 4b). The different ages are in agreement with the locations of the geologic units, with the oldest glacial surfaces at the largest distance from the southeastern part of the depressions, and the youngest surface in the interior of depression A. The error inherent to this technique is ±30% (vertical black lines are error bars). **b**, Changes in the obliquity of Mars' rotational axis over the last 10 Myr (ref. 7). The past ~10 Myr can be reliably modelled despite the chaotic behaviour of the orbits in the Solar System[7,24], so the large increase in obliquity at ~5 Myr is robust. The youngest crater model age derived from our crater counts is plotted as a broad arrow on top of the figure (the other ages fall outside the range shown here). The width of the arrow corresponds to the 30% uncertainty. Note that all our ages are older than the abrupt increase of obliquity at 5 Myr. Our age measurements suggest that the mean obliquity might have been higher than today even before 10 Myr ago, allowing ice to be present globally according to climate models[6].

although there is a hydrogen-rich zone at Elysium[22], the spatial resolution of these measurements is far too low to detect any local enrichment on the scale of the landforms seen at Hecates Tholus. At present, the pressure and temperature conditions of the martian atmosphere prevent near-surface ice from being stable at equatorial latitudes[6]. However, the obliquity of the planet's rotational axis varied significantly over the past 20 Myr (ref. 7). In periods of higher obliquity the climate was different from today's[23].

According to recent climate models, north polar water-ice could be mobilized under such conditions[24] and be deposited at mid- and low latitudes[25,26] where it would have been stable[6]. This study is the first to combine calculations of orbital variations and climate models with the absolute dating of glacial surface features. The ages of glacial deposits on Hecates Tholus range from 25 to 5 Myr before present, with a ±30% error (Fig. 4a). This corresponds very well to a period of increased obliquity, which ended about 5 Myr ago[7] (Fig. 4b). The averaged long-term obliquity between 5 and 20 Myr ago is >35°, a value that is predicted by models to allow ice to be stable globally[6]. Hence, our observations show that the independent results on orbital variations[7] and climate modelling[24–26] are in chronological agreement with geologic surface features.

There are several reasons why ice may still be present at Hecates Tholus. The sublimation of ice results in the accumulation of sediment particles at the surface, and the formation of a lag deposit that is very effective in protecting ice from further sublimation[27]. In addition, Elysium is a long-term sink of atmospheric dust[26], the deposition of which might have further decreased the sublimation rate. There is no evidence for significant degradation or for collapse features like kettle holes in images of the interior of depression A (Fig. 3b). We conclude that there may well have been some unknown amount of sublimation, but that ice is still buried and maintains the 'intact' appearance of the surface. On Earth, Miocene-aged ice (~8 Myr) is still present in the Antarctic dry valleys under a layer of sublimation till[28]. Therefore, the ice at Hecates Tholus may well have been preserved in very shallow depths for geologically long timescales[29,30], and could even be present today and accessible for automated or human exploration. □

Received 3 September 2004; accepted 2 February 2005; doi:10.1038/nature03423.

1. Greeley, R. & Spudis, P. D. Volcanism on Mars. *Rev. Geophys. Space Phys.* **19,** 13–41 (1981).
2. Mouginis-Mark, P. J., Wilson, L. & Zuber, M. T. in *Mars* (eds Kieffer, H. H., Jakosky, B. M., Snyder, C. W. & Matthews, M. S.) 424–452 (Univ. Arizona Press, Tucson/London, 1992).
3. Francis, P. W. & Wood, C. A. Absence of silicic volcanism on Mars: Implications for crustal composition and volatile abundance. *J. Geophys. Res.* **87,** 9881–9889 (1982).
4. Wilson, L. & Head, J. W. Mars: review and analysis of volcanic eruption theory and relationships to observed landforms. *Rev. Geophys.* **32,** 221–263 (1994).
5. Greeley, R. & Crown, D. A. Volcanic geology of Tyrrhena Patera, Mars. *J. Geophys. Res.* **95,** 7133–7149 (1993).
6. Mellon, M. T. & Jakosky, B. M. The distribution and behaviour of martian ground ice during past and present epochs. *J. Geophys. Res.* **100,** 11781–11799 (1995).
7. Laskar, J. *et al.* Long term evolution and chaotic diffusion of the insolation quantities of Mars. *Icarus* **170,** 343–364 (2004).
8. Neukum, G. *et al. HRSC: The High Resolution Stereo Camera of Mars Express* 17–35 (Report ESA-SP-1240, European Space Agency Publications Division, Noordwijk, The Netherlands, 2004).
9. Mouginis-Mark, P. J., Wilson, L. & Head, J. W. Explosive Volcanism on Hecates Tholus, Mars: Investigation of Eruption Conditions. *J. Geophys. Res.* **87,** 9890–9904 (1982).
10. Wewel, F., Scholten, F. & Gwinner, K. High Resolution Stereo Camera (HRSC)—Multispectral 3D-data aquisition and photogrammetric data processing. *Can. J. Remote Sens.* **26,** 466–474 (2000).
11. Werner, S. C., Ivanov, B. A. & Neukum, G. Impact cratering on Mars: Search for target influence on morphology. *Lunar Planet. Sci.* **XXXV,** abstr. 1953 [CD-ROM] (Lunar and Planetary Institute, Houston, 2004).
12. Gulick, V. C. & Baker, V. R. Origin and evolution of valleys on martian volcanoes. *J. Geophys. Res.* **95,** 14325–14344 (1990).
13. Hartmann, W. K. & Neukum, G. Cratering chronology and the evolution of Mars. *Space Sci. Rev.* **96,** 165–194 (2001).
14. Neukum, G. *et al.* Mars: Recent and episodic volcanic and glacial activity on Mars revealed by the High Resolution Stereo Camera. *Nature* **432,** 971–979 (2004).
15. Squyres, S. W. Martian fretted terrain: flow of erosional debris. *Icarus* **34,** 600–613 (1978).
16. Mangold, N. Geomorphic analysis of lobate debris aprons on Mars at Mars Orbiter Camera scale: Evidence for ice sublimation initiated by fractures. *J. Geophys. Res.* **108,** 8021, doi:10.1029/2002JE001885 (2003).
17. Baker, V. R. Water and the martian landscape. *Nature* **412,** 228–236 (2001).
18. Wall, S. W. Analysis of condensates formed at the Viking 2 Lander site: The first winter. *Icarus* **47,** 173–183 (1981).
19. Head, J. W. & Marchant, D. R. Cold-based mountain glaciers on Mars: Western Arsia Mons. *Geology* **31,** 641–644 (2003).
20. Head, J. W., Mustard, J. F., Kreslavsky, A., Milliken, R. E. & Marchant, D. R. Recent ice ages on Mars. *Nature* **426,** 797–802 (2003).

21. Mitrofanov, I. *et al.* Maps of subsurface hydrogen from the high-energy neutron detector, Mars Odyssey. *Science* **297,** 78–81 (2002).
22. Feldman, W. C. *et al.* Global distribution of near-surface hydrogen on Mars. *J. Geophys. Res.* **109,** E09006, doi:10.1029/2003JE002160 (2004).
23. Jakosky, B. M., Henderson, B. G. & Mellon, M. T. Chaotic obliquity and the nature of the martian climate. *J. Geophys. Res.* **100,** 1579–1584 (1995).
24. Levrard, B., Forget, F., Montmessin, F. & Laskar, J. Recent ice-rich deposits formed at high latitudes on Mars by sublimation of unstable equatorial ice during low obliquity. *Nature* **431,** 1072–1075 (2004).
25. Mischna, M. A., Richardson, M. I., Wilson, R. J. & McCleese, D. J. On the orbital forcing of martian water and CO_2 cycles: A general circulation model study with simplified volatile schemes. *J. Geophys. Res.* **108,** 5062, doi:10.1029/2003JE002051 (2003).
26. Haberle, R. M., Murphy, J. R. & Schaeffer, J. Orbital change experiments with a Mars general circulation model. *Icarus* **161,** 66–89 (2003).
27. Skorov, Y. V. *et al.* Stability of water ice under a porous nonvolatile layer: implications to the south polar layered deposits of Mars. *Planet. Space Sci.* **49,** 59–63 (2001).
28. Marchant, D. R. *et al.* Formation of patterned ground and sublimation till over Miocene glacier ice in Beacon Valley, southern Victoria Land, Antarctica. *Geol. Soc. Am. Bull.* **114,** 718–730 (2002).
29. Mellon, M. T., Jakosky, B. M. & Postawko, S. E. The persistence of equatorial ground ice on Mars. *J. Geophys. Res.* **102,** 19357–19369 (1997).
30. Helbert, J. & Benkhoff, J. A new model on the thermal behavior of the near surface layer on Mars and its implications for ground ice deposits in Gusev Crater. *6th Int. Conf. Mars* abstr. 3019 [CD-ROM] (Lunar and Planetary Institute, Houston, 2003).

Acknowledgements We thank the entire HRSC experiment and instrument teams at the German Aerospace Center (DLR) and at the Freie Universität Berlin, as well as the Mars Express teams at ESTEC and ESOC. This study would not have been possible without their work. In particular, we appreciate the support of H. Hoffmann, T. Roatsch, K.-D. Matz, V. Mertens, J. Flohrer, R. Pischel, F. Scholten and K. Gwinner. HRSC was developed at DLR and industrial partners. G.N. is the Principal Investigator of this experiment. We are grateful to U. Wolf for her support in crater counting. M. Aittola, J. Korteniemi, P. Kostama and D. Williams supported the HRSC image planning. T. Lowell provided an image of his collection of glacier photographs. Comments by J. Helbert helped to improve the manuscript.

Competing interests statement The authors declare that they have no competing financial interests.

Correspondence and requests for materials should be addressed to E.H. (Ernst.Hauber@dlr.de).

The HRSC Co-Investigator Team: J. Albertz[1], A. T. Basilevsky[2], G. Bellucci[3], J.-P. Bibring[4], M. Buchroithner[5], M. H. Carr[6], E. Dorrer[7], T. C. Duxbury[8], H. Ebner[9], B. H. Foing[10], R. Greeley[11], E. Hauber[12], J. W. Head III[13], C. Heipke[14], H. Hoffmann[12], A. Inada[15,18], W.-H. Ip[16], B. A. Ivanov[17], R. Jaumann[12], H. U. Keller[18], R. Kirk[19], K. Kraus[20], P. Kronberg[21], R. Kuzmin[2], Y. Langevin[4], K. Lumme[22], W. Markiewicz[18], P. Masson[23], H. Mayer[7], T. B. McCord[24], J.-P. Muller[25], J. B. Murray[26], F. M. Neubauer[27], G. Neukum[28], J. Oberst[12], G. G. Ori[29], M. Pätzold[27], P. Pinet[30], R. Pischel[12], F. Poulet[4], J. Raitala[31], G. Schwarz[32], T. Spohn[12] & S. W. Squyres[33]

Affiliations of authors: 1, TU Berlin, D-10623 Germany; 2, Vernadsky Institute-RAS, Moscow 117975, Russia; 3, IFSI/CNR, 00133 Rome, Italy; 4, IAS, 91405 Orsay cedex, France; 5, TU Dresden D-01062, Germany; 6, USGS, MS 975 Menlo Park, California 94025, USA; 7, Universität der Bundeswehr München D-85577, Germany; 8, JPL, Pasadena, California 91109, USA; 9, TU München D-80333, Germany; 10, ESTEC/SCI-SR, Postbus 299, NL-2200 AG Noordwijk, The Netherlands; 11, Arizona State University, Box 871404, Tempe, Arizona 85287-1404, USA; 12, DLR, Berlin D-12489, Germany; 13, Brown University, Box 1846, Providence, Rhode Island 02912, USA; 14, Universität Hannover, D-30167, Germany; 15, Kobe University, 657-8501 Kobe, Japan; 16, National Central University (NCU), Chung-Li 320, Taiwan; 17, IDG-RAS, Moscow 117979, Russia; 18, MPS, Postfach 20, D-37191, Germany; 19, USGS, Flagstaff, Arizona 86001, USA; 20, TU Wien A-1040, Austria; 21, TU Clausthal D-38678, Germany; 22, University of Helsinki, PO Box 14, SF-00014 Finland; 23, OrsayTerre, F-91405 Orsay cedex, France; 24, PSI-Nw, Winthrop, Washington 98862, USA; 25, University College London WC1E 6BT, UK; 26, The Open University, Milton Keynes MK7 6AA, Buckinghamshire, UK; 27,Universität Köln, D-50923, Germany; 28, FU Berlin D-12249, Germany; 29, IRSPS, I-65127 Pescara, Italy; 30, Observatoire de Midi-Pyrénées, F-31400 Toulouse, France; 31, University of Oulu, FIN-90401, Finland; 32, DLR, D-82234 Wessling, Germany; 33, Cornell University, Ithaca, New York 15853-1301, USA

Current measurement by real-time counting of single electrons

Jonas Bylander, Tim Duty & Per Delsing

Department of Microtechnology and Nanoscience (MC2), Chalmers University of Technology, SE-412 96 Göteborg, Sweden

The fact that electrical current is carried by individual charges has been known for over 100 years, yet this discreteness has not been directly observed so far. Almost all current measurements involve measuring the voltage drop across a resistor, using Ohm's law, in which the discrete nature of charge does not come into play. However, by sending a direct current through a microelectronic circuit with a chain of islands connected by small tunnel junctions, the individual electrons can be observed one by one. The quantum mechanical tunnelling of single charges in this one-dimensional array is time correlated[1–3], and consequently the detected signal has the average frequency $f = I/e$, where I is the current and e is the electron charge. Here we report a direct observation of these time-correlated single-electron tunnelling oscillations, and show electron counting in the range 5 fA–1 pA. This represents a fundamentally new way to measure extremely small currents, without offset or drift. Moreover, our current measurement, which is based on electron counting, is self-calibrated, as the measured frequency is related to the current only by a natural constant.

In the mid-1980s, it was suggested[1] that a small current consisting of individual electrons, tunnelling through a small tunnel junction, could at low temperatures result in an oscillating voltage of amplitude e/C, where C is the capacitance of the tunnel junction. The full theory for these so-called single-electron tunnelling oscillations was then developed[2], based on earlier work on Bloch oscillations and the underlying Coulomb blockade[4,5]. This phenomenon of single-electron tunnelling oscillations is similar to the a.c. Josephson effect, as phase and charge are quantum conjugated variables. However, the duality is not complete because the single-electron tunnelling oscillations are lacking coherence. A few years later, these oscillations were detected indirectly by phase locking to an external microwave signal[6]. Shortly thereafter, new devices such as the single-electron turnstile[7] and the single-electron pump[8] were invented in order to create a current given by the fundamental relation $I = ef$. Since then, the single-electron pump has been refined to a very high accuracy[9].

A number of authors have also proposed[10–13] that it should be possible to turn this relation around, and instead measure the current by monitoring the individual electrons as they pass through a circuit. More recently, single-electron tunnelling events have been observed[14,15]. In those experiments, however, there was no time correlation, and thus no relation between frequency and current could be demonstrated.

In order to measure current by electron counting, three main ingredients are necessary: time correlation of the tunnelling events, a fast and sensitive charge detector, and a very stable current bias. To bring about time correlation in a single tunnel junction, in contrast to uncorrelated shot noise[16], care must be taken to make the electromagnetic impedance seen by the junction large[2] compared to the Klitzing resistance, $R_K = h/e^2 \approx 25.8\,\mathrm{k\Omega}$. This can be achieved by placing small-size resistors in close proximity to the junction[17,18] or by using a one-dimensional series array of tunnel junctions[19].

In our experiment, we have used a superconducting array containing $N = 50$ junctions (Fig. 1). The capacitance of each junction is $C_A \approx 0.42\,\mathrm{fF}$, and the stray capacitance of an electrode inside the array is $C_0 \approx 30\,\mathrm{aF}$. In such an array, excess charge on one island polarizes the neighbouring islands, so that the charges repel each